Karin Sigl, BSc

Non-hydrolytic cellulose-binding proteins

MASTER'S THESIS

to achieve the university degree of

Diplom-Ingenieurin

Master’s degree program: Biotechnology

Submitted to:

Graz University of Technology

Supervisor:

Univ.-Prof. Dipl.-Ing. Dr. techn. Bernd Nidetzky

Graz, June 2015

AFFIDAVIT

I declare that I have authored this thesis independently, that I have not used other than the declared sources/resources, and that I have explicitly indicated all ma- terial which has been quoted either literally or by content from the sources used. The text document uploaded to TUGRAZonline is identical to the present master‘s thesis dissertation.

Date

Signature

Acknowledgements

First and foremost I want to express my sincere gratitude to my diploma supervisors Univ.-Prof. Dipl.-Ing. Dr. techn. Bernd Nidetzky and Dipl.-Ing. Manuel Eibinger for their encouragement and excellent guidance and support throughout my time at the institute.

I want to thank the whole team of the Institute of Biotechnology and Biochemical Engineering for any help in the laboratory and the good time I had.

Special thanks are given to Dipl.-Ing. Dr. techn. Harald Plank, Dipl.-Ing. BSc Thomas Ganner und Dipl.-Ing. BSc Jürgen Sattelkow from the Institute of Electronmicroscopy and Nanoanalysis for their great cooperation and valuable contribution to the project by making hidden structures visible.

I also want to thank Dr. rer. nat. Bernhard Seiboth and his group from Vienna University of Technology for providing us with *T. reesei* supernatant, and from University of Graz I want to thank Dipl.-Biol. Dr. rer. nat. habil. Christian Berg for different kinds of grass sorts provided and Christian Fercher, MSc, for his guidance in the circular dichroism measurement.

My friends have been more than support throughout the last months. I especially want to thank Caroline and Melitta for awesome 15 years of inspiration, laughs and friendship and Stefan for making my world better.

Infinite gratitude I owe my parents Sonja and Martin and my siblings Lisa and Matthias – my dearest critics and greatest cheerleaders.

For my family

Content

Manuscript Draft – *Trichoderma reesei* SWO1: Biochemical and structural assessment and new findings about its activities on lignocellulose

Abstract

Cellulose remains the bottleneck of lignocellulose degradation and, therefore, the limiting step in the production of second generation biofuels. Among other factors, cellulose recalcitrance and insolubility contribute most to enzymatic resistance. A protein-performed way to improve the accessibility of cellulose and by that to increase the cellulosic breakdown has been lately addressed by several research groups and has been met with great response. Special non-hydrolytic proteins have the ability to bind and alter lignocellulose, like the *Trichoderma reesei* SWO1. They depend on a process named amorphogenesis, which is proposed to weaken cellulose chain interaction and to cause swelling and loosening of cellulose without the release of reducing sugars. In our study we investigated its structural and biochemical properties and examined its activity on pure cellulosic substrates and natural lignocellulosic material. We could conclude that SWO1 does not have an amorphogenesis effect on pure cellulose, but might work as an accessory protein on natural non-treated substrates.

Introduction

The steadily increasing need for sustainable and competitive biofuels is pushing research to find innovative and efficient ways to meet the demands. In the last decades there has been much effort to develop a feasible production process for second generation biofuels – the generation of petrochemicals from lignocellulosic raw materials [1]. Despite these ambitions, cellulose recalcitrance remains the main bottleneck for an efficient bioprocess [2,3].

Lignocellulose as part of cell walls is an adept invention of nature – a mechanically and chemically highly resistant material that protects plants and gives them structure [4]. Its core component is cellulose, the most abundant biopolymer in nature. Cellulose is further stabilized by hemicellulose, a material that consists of branched, acetylated hexose and pentose units [5], and lignin, a phenolic polymer that binds covalently to hemicellulose, by that strengthening the lignocellulosic structure [6].

In comparison to cellulose hemicellulose and lignin are easily degraded. Nevertheless, their processing to valuable products is limited due to the fact that xylose-metabolizing organisms show low productivities and genetically engineered producers are currently at the level of development [7–9]. In the case of lignin the heterogeneity is a factor that makes the manufacture of beneficial goods difficult [10]. The production of second-generation biofuel starts with the breakdown of lignocellulosic material like waste from the paper industry or from agriculture [11–13]. To extract the cellulosic raw material a number of different pre-treatments have been investigated and tested, including chemical, mechanical and thermic methods [14–27]. These pre-treatments aim to degrade hemicellulosic and lignin presenting parts as well as to partially loosen the recalcitrant structure of cellulose. The efficient breakdown of remaining cellulose has been the subject of investigation for many research groups over the past decades. Cellulose consists of homopolymeric unbranched β-1,4-linked D-glucose units with a polymerization grade from several hundred to over 10.000. Each glucose unit is rotated by 180° relative to its neighbouring unit, resulting in a straight cellulose chain. 30 to 36 of these chains form microfibrilic structures held together by hydrogen bonds and van der Waals forces. These structures form larger fibrils with other chain bundles. In summary, it is the current opinion that the rotation and stacking on the one hand and the binding and interaction of cellulose chains on the other hand are the reason for a relatively restricted accessible area [28–30], which causes the highly resistant characteristic to enzymatic degradation on cellulose [31–35].

There are two types of cellulase systems known in nature. The bacterial cellulosome is a large multi-protein complex that consists of a cell wall-anchored scaffold associated with cellulases [36,37]. The fungal cellulase system on the other hand consists of single secreted cellulases that act together on the cellulosic surface. The main enzymes of this cellulase system are exo-acting Cellobiohydrolase I and II (CBH I and II) that cleave off cellobiose-units from reducing and non-reducing ends, respectively, as well as several Endoglucanases (EG) that cut within the cellulose-chains [38,39]. Also, β-Glucosidases are of vital importance in the cellulase system, because they cleave the inhibitory cellobiose into glucose. An interesting feature of this kind of cellulase system is that their overall degradation performance is higher together than the sum of their single hydrolysis products [38,39].

Also, such an effect has been reported for non-hydrolytic proteins and has been met with great response [40–44]. It has been found for several types of proteins, for example expansins and expansin-like proteins [45]. They depend on a process named amorphogenesis [40], which has been proposed to weaken cellulose chain interaction and to cause swelling and loosening of cellulose without the release of reducing sugars. This process extends the accessible surface of cellulose and weakens the fibrillose structure. By that amorphous areas are introduced into the otherwise crystalline structure, which enhances the accessibility for hydrolytic enzymes and results in an increased degradation of cellulose [42]. Synergism has recently been reported for the bacterial expansins *Bacillus pumilus* BpEX and *Clavibacter michiganensis* CmEX on Avicel – a crystalline cellulose –, arabinoxylan and phosphoric acid-swollen cellulose (PASC) together with a commercially available cellulase mix [46]. Additionally, cellulases in interaction with *Bacillus subtilis* EXLX1 showed an increased release of sugars when incubated with filter paper [47]. In the fungal kingdom synergism effects with expansin-like proteins like *Aspergillus oryzae* ELP1 and *Trichoderma reesei* SWO1 have been reported [48]. Especially *T. reesei* SWO1 has aroused much attention in the last years. Reports on a swelling effect of filter paper, cotton fibers and *Valonia* cell wall fragments by an engineered *Saccharomyces cerevisiae* expressed

Swollenin [49], the swelling of cotton fibers by a *Nicotiana tabacum* and *E. coli* expressed Swollenin [50] and a dispersion of cotton fibers by a *Kluyveromyces lactis* expressed, HIS-tagged and secretion signal sequence-truncated Swollenin [51] gave rise to high expectations of this protein to have distinct amorphogenesis introducing properties. Moreover, there are several reports on synergism effects of differently expressed *T. reesei* Swollenin with cellulases and xylanases, like synergism with a cellulase mix on filter paper, Avicel and α-Cellulose [51], synergism with a single endoglucanase and different endo-xylanases on steam pretreated corn stover [52] and synergism with a single endoglucanase on filter paper [53]. All mentioned Swollenin proteins have either been modified [51,52] and/or expressed in heterologous host strains like *Pichia pastoris* [53].

Although there have been several reports on synergism effects observed, the described effects of some reports could not be reproduced, indicating controversy in the literature. For example, Gourlay et al. (2013) [52] reported that Swollenin did not show any synergism effects with different cellobiohydrolases (CBH), while others reported that Swollenin showed no amorphogenesis effect on substrates like carboxymethyl cellulose, 4-Nitrophenyl-beta-D-glucopyranoside, microcrystalline cellulose, oat spelt xylan, and glucomannan [50]. In our study we aim to further contribute to the knowledge of SWO1 properties and to find out more about its impact on pure cellulosic substrates and natural lignocellulosic material.

Materials and methods

Overall protein-content in *T. reesei* RUT C-30 supernatant and purification of SWO1

T. reesei RUT C-30 supernatant was kindly provided by Bernhard Seiboth and his group from Vienna University of Technology. The overall-content of protein in *T. reesei RUT C-30*

supernatant was determined by UV-absorption on a Nanodrop system (DS-II+Spectrometer, DeNovix) with an absorption of 1 for 1 g/l (ProtParam) at 280 nm.

SWO1 (Accession number in UniProt: Q9P8D0) was isolated from the supernatant using an affinity chromatography. 50 ml of *T. reesei* RUT C-30 supernatant were incubated with 0.75 g Avicel (PH-101, Sigma Aldrich) in 50 ml of 50 mM sodium acetate buffer pH 5.0 (reaction buffer) in a beaker at 200 rpm on an RCT basics hotplate (IKA) for 2 h at room temperature. This mixture was transferred into 50 ml Falcon tubes (Sarstedt) and centrifuged at 5000 rpm for 5 min at 4 °C. The pellets were combined and resuspended in 10 ml of reaction buffer, while the supernatant was discarded. The mixture was loaded onto a disposable 10 ml polypropylene affinity column (ThermoScientific), washed twice with reaction buffer and once with ddH_2O. Subsequently, SWO1 was eluted with 1 % triethylamin (TEA, Sigma Aldrich) and collected in 15 ml Falcon tubes (Sarstedt). TEA removal, adjusting to reaction buffer and SWO1 concentration were carried out in one step by centrifugation in spin filter columns (Vivaspin Turbo, Vivaspin 6, Sartorius AG) at 5000 rpm and 4 °C.

The protein concentration was determined by UV-absorption on a Nanodrop system with a calculated absorption of 1.704 for 1 g/l (ProtParam) at 280 nm and the purification was evaluated with SDS-PAGE, using a protein marker for the evaluation of proteins with a molecular weight of 10-200 kDa (peqGOLD Protein Marker II, peqlab).

Circular dichroism (CD) and modelling

Circular dichroism spectra were assessed on a Jasco J-175 spectropolarimeter using a 10 mm cylindrical quartz cell. SWO1 was used at a concentration of 0.1 mg/ml in reaction buffer. The baseline of the spectra was obtained from pure reaction buffer. The standard parameters for protein evaluation were chosen with a sensitivity of 100 mdeg, a start wavelength of 250 to 320 nm, an end wavelength of 190 to 250 nm and a data pitch of 1 nm. For good data quality a slow

scanning mode with a continuous scanning speed of 10 nm/min was chosen. The combined spectra were evaluated online with DichroWeb.

Furthermore, a modelling approach was employed: The amino acid sequence of SWO1 was uploaded to Phyre2 and its 3D structure could be evaluated.

Adsorption experiments

The binding of SWO1 was determined on 1 mg/ml Avicel, birch wood xylan (ROTH) and lignin (alkali, Aldrich) at concentrations of 0.2 – 25 µM of SWO1 in reaction buffer with a working volume of 50 µl. SWO1 was incubated with the substrate in 1.5 ml reaction tubes (Sarstedt) on a thermomixer (Eppendorf) at 25 °C and 500 rpm. After 2 h the samples were centrifuged for 5 min at 13.000 rpm and 4 °C to segregate substrate-bound SWO1 and the supernatant was transferred into new 1.5 ml tubes. The experiments were carried out in duplicates and the protein concentration of the supernatant was determined by BCA (Thermo Scientific) (Avicel) and Roti-Nanoquant (ROTH) (xylan, lignin) according to the instructions of the manufacturer and with a *T. reesei* cellobiohydrolase 1 (CBH1) standard in the range of 20-200 µg/ml. CBH1 was produced conforming to Medve (1998) [54].

For the calculation of bound protein the following formula was employed: *Protein added [µM] - Protein in supernatant [µM] – Protein in substrate control [µM] = Bound Protein [µM]*

Activity of SWO1 on pure cellulosic substrates

0.4 µM SWO1 and bovine serum albumin (BSA, Thermo Scientific) as a control were incubated with 1 mg/ml Avicel or nanocrystalline cellulose (NCC), respectively, in reaction buffer with a working volume of 500 µl at 40 °C and 500 rpm on a thermomixer. 200 µl samples were taken when starting the incubation and again after 10 and 24 h. They were boiled at 95 °C for 10 min, centrifuged for 1 min at 13.000 rpm and the supernatant was transferred into new 1.5 ml tubes. The experiments were carried out in four replicates and with a separate sample at each time

point. The released glucose concentration was measured using GOD-POD accordingly to Wildberger et al. (2011) [55], an assay containing hexokinase and glucose-6-phosphate dehydrogenase. A glucose calibration standard (Analyticon) in the range of 0.01-1 mM was used. NCC were produced according to the method of Habibi et al. (2010) [56].

Similar conditions were used when treating cellotetraose (Carbosynth) with SWO1. However, the SWO1 concentration was changed to 0.5 µM and the substrate concentration to 0.5 mg/ml. The reaction was stopped by adding 100 mM NaOH (Merck) to 100 µl sample. Since we wanted to assess the amount and proportion of all reducing sugars formed, we used a Dionex system (BioLC) with an ED50 electrochemical detector, a GS50 gradient pump and an AS50 autosampler using a Dionex CarboPac PA10 column for monomeric and short-chain sugars.

To calculate the released amount of reducing sugars by Avicel, NCC and tetracellulose the following formula was employed: *(Glucose in supernatant [µM] – Glucose in supernatant of substrate control [µM]) / Substrate added [µM] *100 = Released glucose [%],* corrected with the dilution factor of NaOH.

Activity of SWO1 on β-glucan

The assessment of activity of 0.2 µM SWO1 was performed on 1 mg/ml barley β-glucan (high viscosity >100 cST, Megazyme) in reaction buffer with a working volume of 250 µl at 40 °C and 500 rpm on a thermomixer. 100 µl samples were taken when starting the incubation and again after 24 h. The reaction was stopped by adding 100 µl of 100 mM NaOH. To remove solids the samples were centrifuged for 3 min at 13.000 rpm. The supernatants were transferred into new 1.5 ml tubes. The experiments were carried out in duplicates and with BSA as a reference. The amount of released sugars was evaluated by a Dionex system with an ED50 electrochemical detector, a GS50 gradient pump and an AS50 autosampler using a Dionex CarboPac PA10 column for monomeric and short-chain sugars. For the calculation of released glucose [%] the

formula from sub-chapter *activity measurements on pure cellulosic substrates* was used and corrected with the dilution factor of NaOH.

Evaluation of synergism effects with SVG on pure cellulosic substrates

Determination of synergism of SWO1 with a complete cellulase mixture from *T. reesei* strain SVG 17 (SVG, 1 FPU/ml) was performed on Avicel and NCC. SVG was obtained following the method by Eibinger et al. (2014) [57].

The first step included a pre-incubation of 1 mg/ml Avicel or NCC with 0.4 µM SWO1 for 24 h at 40 °C and 500 rpm on a thermomixer in reaction buffer with a working volume of 500 µl. The same conditions were used for the following hydrolysis, which was induced by adding 20 µg SVG per mg substrate. Moreover, 2 µl of an *Aspergillus niger* β-glucosidase (40 U/ml, Megazyme) were added to avoid inhibitory effects of cellobiose on the cellulases. 150 µl samples were taken after 0 min, 30 min, 45 min, 60 min, 90 min, 120 min and 24 h. They were boiled at 95 °C, vortexed and centrifuged for 1 min at 13.000 rpm and 4 °C. The amount of released glucose was determined in the supernatant by GOD-POD and using a glucose calibration standard in the range of 0.01-1 mM. The experiments were done in four replicates and for the calculation of released glucose [%] the formula from sub-chapter *activity measurements on pure cellulosic substrates* was used.

Determination of altered substrate properties after SWO1 treatment

Atomic force microscopy (AFM)

In situ data of substrate surfaces could be obtained by a FastScanBio AFM (Bruker Nano) in a micro-fluid cell in reaction buffer at 40 °C and a Nanoscope 9.1 Controller. The substrate surfaces were determined in TappingMode with a FastScanA cantilever (Bruker Nano). Scan rates, set points and drive amplitude were adapted to a gentle tapping interaction of tip and sample. *In situ* AFM imaging of the structural changes upon protein activity was carried out with

0.4 µM SWO1 on C2 (amorphous cellulose)- and NCC-coated silica discs. The amorphous cellulose was prepared accordingly to O'Sullivan et al. (1997) [58]. To evaluate the impact of SWO1 on the substrates images of their surface were collected before and after 24 h of incubation with 0.4 µM SWO1. A scan size of 1 x 1 µm² and resolution of 512 x 512 pixels was chosen. The recorded AFM images were processed and analyzed using GWYDDION (V2.31), Origin 9 (OriginLab) and NANOSCOPE ANALYSIS 1.20 (Build R1Sr3.64571, Veeco Instruments) software in order to quantify the visualized features.

Wide-angle x-ray scattering (WAXS)

Wide-angle x-ray scattering analysis (WAXS) was carried out on a Siemens D 5005 diffractometer (Siemens) using CuKa (0.154 nm) radiation at 40 kV and 40 mA. 10 mg/ml Avicel were incubated with 0.01 µM SWO1 for 72 h in a shaking water bath (GFL 1083) at 150 rpm. As a reference Avicel without SWO1 incubation was used. The probes were dried at 60 °C overnight, and were put on a zero diffraction silicon crystal holder (Bruker AXS). All samples were characterized in locked coupledH/2Hmode from 10_ to 60_ (2H) with an angle increment of 0.05_ in 6 s. Data analysis was performed using Origin 9. Deconvolution was performed by the Nonlinear Curve Fit tool (Origin 9, OriginLab) via gauss functions. Peak positions where held fixed for the 1,483 cm-1 (crystalline) band to gain the corresponding intensities.

Evaluation of synergism effects of SWO1 with SVG on dried grass

1 mg/ml of *Dactylis glomerata* grass, which was first dried at 80 °C overnight, was incubated with 0.02 µM of SWO1 or BSA as a reference and 2 µg SVG per mg dried grass on a thermomixer at 40 °C and 500 rpm in reaction buffer with a working volume of 1 ml. 100 µl samples were taken after 164 h. The reaction was stopped by adding 100 µl of 100 mM NaOH. The samples were vortexed and centrifuged for 3 min at 13.000 rpm and 4 °C and the supernatants were transferred into new 1.5 reaction tubes. The amount of released glucose in the supernatant was determined by DNS employing the method of Xiao et al. (2004) [59] and using a standard with 4-

12 mM glucose. The experiments were done in duplicates and for the calculation of released glucose [%] the formula from sub-chapter *activity measurements on cellulosic substrates* was used and corrected with the dilution factor of NaOH.

Results and discussion

Purification of SWO1

T. reesei RUT C-30 is a genetically engineered strain, which is commonly used in the laboratory [60]. Its secretory cellulases have been knocked out resulting in a cellulase-free supernatant that contains other secretory proteins, among them SWO1 [60]. In this study a yield of 4 mg/l (wet weight) SWO1 from *T. reesei* supernatant could be achieved by affinity chromatography. Since the product shows only little contamination (Fig 1) and, furthermore, the overall content of protein in pure *T. reesei* supernatant is 47 mg/l, determined by UV-absorption, we consider 4-5 % (w/w) SWO1 in the genetically engineered *T. reesei* RUT 30 supernatant protein as realistic. This value is further emphasized by comparing the intensity of SDS-bands of *T. reesei* supernatant (Fig 1).

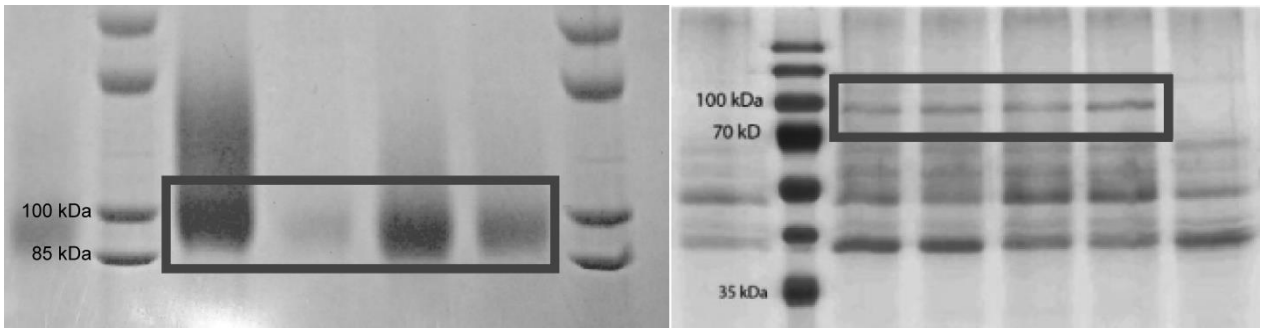

Figure 1. SDS-PAGE: Left: Purification of SWO1: Lane S: Protein standard; Lane 1-4: SWO1 bands isolated from *T. reesei* supernatant are indicated by the rectangle; Right: Complete supernatant of *T. reeisei:* Lane S: Protein standard; Lane 1-4: Bands of proteins as part of the supernatant. Among them SWO1, indicated by the rectangle.

Structural analysis of SWO1

SWO1 exhibits a similar set-up as fungal cellulases. It comprises an N-terminal carbohydrate binding family 1 domain (CBD I), a heavily glycosylated linker and a C-terminal Expansin-like domain [1] with an Endoglucanase 45 (EG 45) core (Blast-research), though it has no efficient catalytic activity. The molecular weight of SWO1 is 51.5 kDa for the non-glycosylated form and an estimated 91 kDa for the glycosylated form (compare Fig 1B). This is in line with typical fungal cellulases, which have a molecular weight of 48-55 kDa (UniProt). Fig 2 shows the predicted model of SWO1 with the 3D-structure determining program Phyre2. It contains the mentioned 3-domain structure. The CD-results evaluated with DichroWeb give additional evidence for the validity of the proposed model (Fig 3). It shows that SWO1 comprises 40 % beta sheets and a minor helical portion of 7 % (Tab 1). We assume that the unstructured part in the evaluation with 34 % is due to the long linker of SWO1.

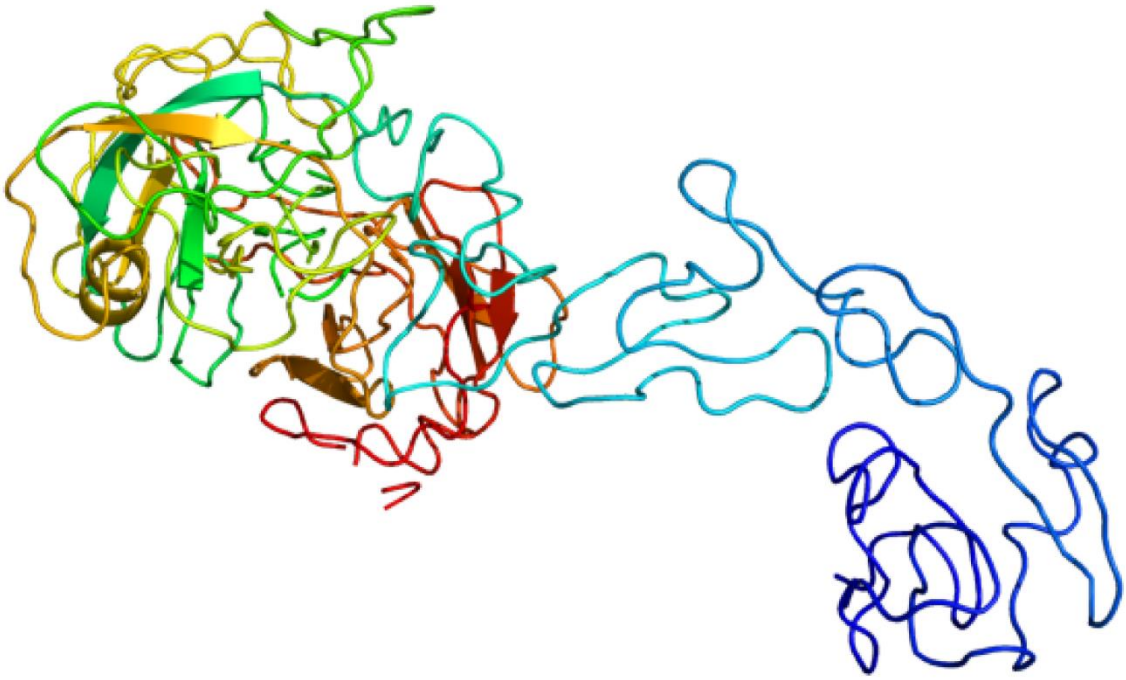

Figure 2 Model of SWO1: It comprises a CBD I, a linker and a catalytic-like structure (from right to left).

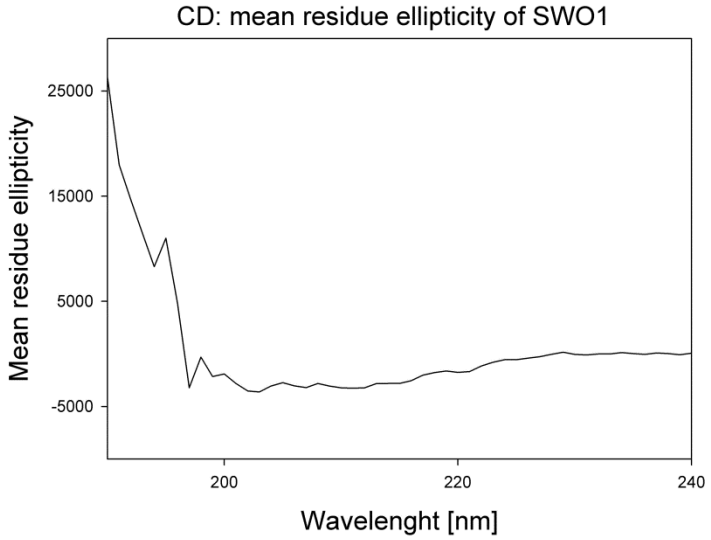

Figure 3 CD measurement: Mean residue ellipticity, which is used to calculate the amount of SWO1 secondary structure elements.

Table 1 Calculated secondary structure elements of SWO1

Helix	7 %
Strand	40 %
Turns	18 %
Unordered	34 %
Total	99 %

Adsorption experiments

The affinity of SWO1 for Avicel (Fig 4A), k_d = 0.89 µM, is comparable to values for Swollenin affinity in the literature [51] and other expansin-like proteins [46]. In comparison to CBD I comprising cellulases SWO1 affinity to Avicel is four to five times higher [61]. It also exhibits an affinity for lignin, kd = 0.52 µM, in the same range (Fig 4C). In addition, SWO1 shows an increased binding to xylan (Fig 4B), k_d = 0.08 µM, which is nearly an order of magnitude higher than for Avicel and lignin. Possible reasons for this increased affinity might be the better accessibility to xylan [62] in comparison to recalcitrant Avicel [23,63] and heterogeneous lignin [10] or better binding properties of SWO1 for this substrate.

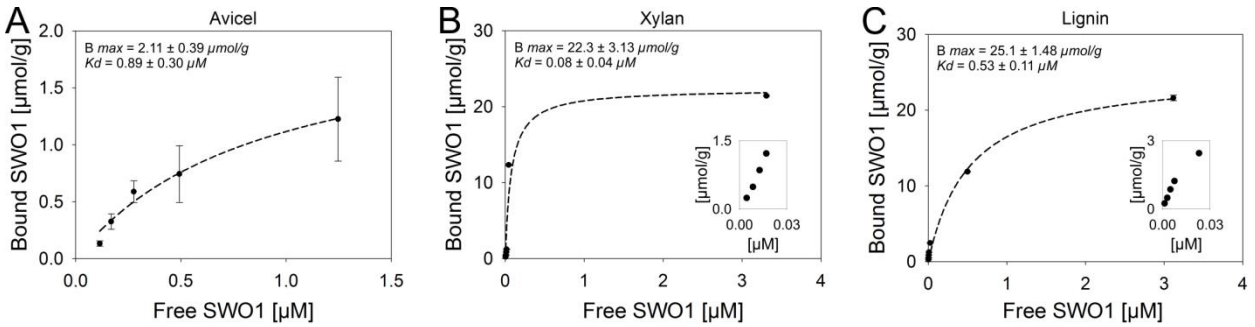

Figure 4 Binding of SWO1 to different substrates. Binding of different concentrations of SWO1 to A) Avicel, B) xylan and C) lignin. Moreover, the initial binding of SWO1 is shown for xylan and lignin.

Activity measurements of SWO1 on pure cellulosic substrates and β-glucan

SWO1 incubation with Avicel and NCC resulted in a release of a minor portion of glucose (Fig 5). In comparison to BSA - which did not show any release of glucose apart from a constant level determined in every probe, probably attributable to a non-specific breakdown - SWO1 shows a small, though significant activity on both Avicel and NCC. A similar degradation showed SWO1 on β-glucan (Fig 6). Surprisingly, a high degradation of cellotetraose (Fig 7) could be obtained. The results correspond well to findings by Andberg et al. (2015) [64], who proposed an endoglucanase-like function coupled with a cellobiohydrolase cleaving mechanism. To further evaluate the mechanism of SWO1 on oligocellulosic substrates further investigations would be necessary.

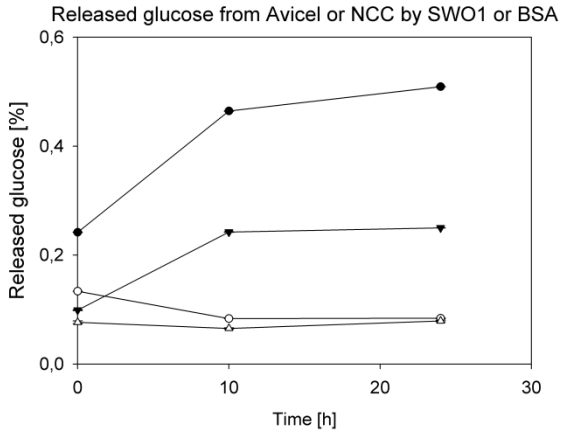

Figure 5 Percentage of released glucose after 24 h of 0.4 µM SWO1 and BSA incubation of 1mg/ml substrate. •SWO1 on Avicel; ○BSA on Avicel; ▼SWO1 on NCC; ∆BSA on NCC.

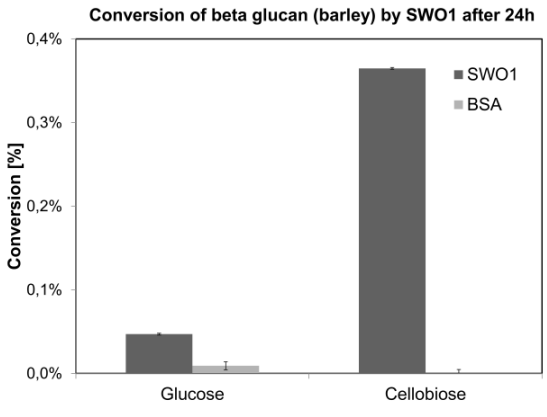

Figure 6 Percentage of released glucose and cellobiose after 24 h incubation of 1 mg/ml barley β-glucan with 0.2 µM SWO1.

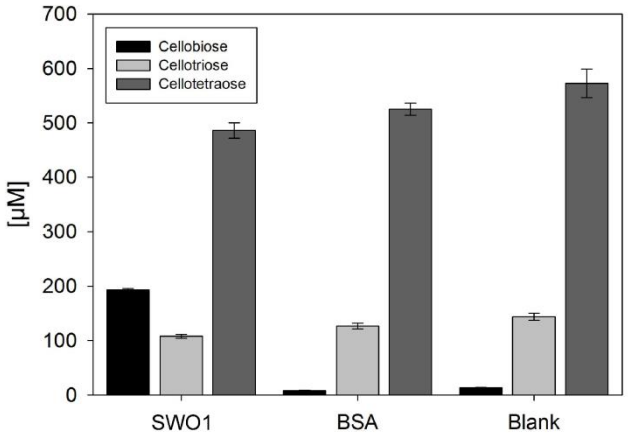

Figure 7 Conversion of 0.5 mg/ml tetracellulose after an incubation of 24 h with 0.5 µM SWO1.

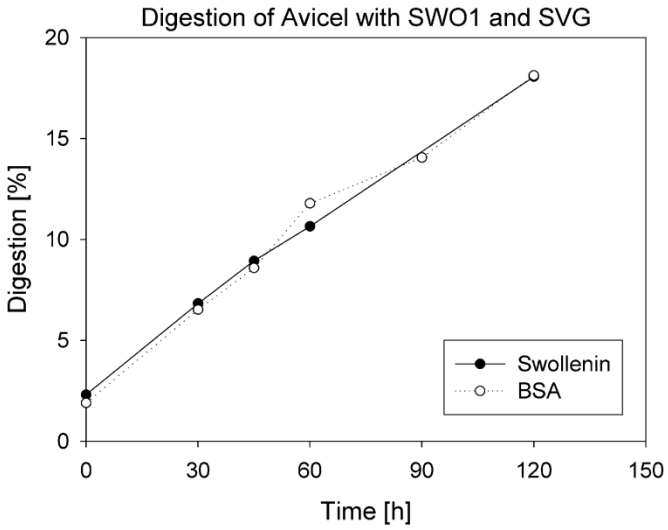

Figure 8 Digestion of 1 mg/ml Avicel of 0.4 µM SWO1- and BSA-pre-treated Avicel with 20 µg SVG per mg substrate.

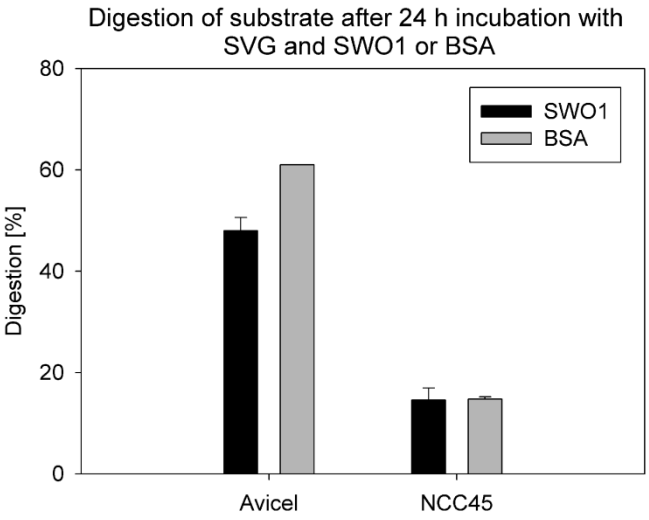

Figure 9 Digestion of 1 mg/ml cellulosic substrate of 0.4 µM SWO1- and BSA-pre-treated Avicel with 20 µg SVG per mg substrate.

Evaluation of synergism effects with SVG on pure cellulosic substrates

It has been proposed that SWO1 has the function of an accessory protein to lignocellulose [49–52]. Since reports of synergism effects on Avicel with fungal cellulases exist [51], we aimed to find out in detail about the mechanism of SWO1 on pure cellulosic substrates. We pre-treated Avicel with SWO1 for 24 h and, after that, measured the initial degradation with SVG. Fig 8 shows that SWO1- and BSA-pre-treated Avicel is degraded at the same rate. Furthermore, an evaluation of SVG-induced degradation of SWO1-pre-treated Avicel and NCC in comparison to a BSA-reference was carried out (Fig 9). All measurements were done in four replicates. Our data show that SWO1 pre-treated NCC does not show synergism with fungal cellulases. After 24 h 14 % of SWO1 and BSA pre-treated NCC, respectively, were degraded by the fungal

cellulases. Moreover, when Avicel was pre-treated with SWO1, the influence was even negative in comparison to BSA pre-treated samples. This result stands in contrast to Jäger et al. (2011) [51]. We propose that SWO1 adsorbs to cellulose, by that inhibiting CBH- and EG- binding sites for an effective degradation. Nevertheless, Jäger et al. (2011) [51] used higher SWO1 concentrations on the substrates than our group did, so this factional situation defies any explanation on our site at the moment.

Determination of altered substrate properties after SWO1 treatment by AFM and WAXS

A visualization method using atomic force microscopy (AFM) and wide angle x-ray scattering (WAXS) were employed to complete our evaluation of possible effects of SWO1 on pure cellulosic substrates. AFM is an effective method to visualize cellulosic surfaces *in-situ* as well as for the evaluation of height profiles on meso- and nano-scale. It has recently been used to track enzymatic degradation of cotton fibres and MACS by fungal cellulases [57,65,66]. We aimed to evaluate, whether SWO1 incubation had an effect on the cellulosic surface. MACS incubated with SWO1 for 24 h did not yield a significant effect (Fig 10). Comparing the image as well as the height distribution of MACS (bright region) before and after the incubation with SWO1, we could show that SWO1 does neither show swelling or loosening of cellulose nor exhibit a degradation as reported [51].As a reference for the height a silica layer (dark region) was used.

Another experiment showed similar results. This time NCC was incubated with SWO1 or BSA, respectively. NCC is highly recalcitrant cellulose consisting of needle-like polymers with a length of 100-200 nm and a width of 3-70 nm depending on the cellulose source and it can be manufactured by treating cellulose fibers with sulfuric acid [56]. The length and width distribution of NCC was compared before and after 24 h of incubation (Fig 11). The data showed no significant differences in SWO1- and BSA-treated NCC.

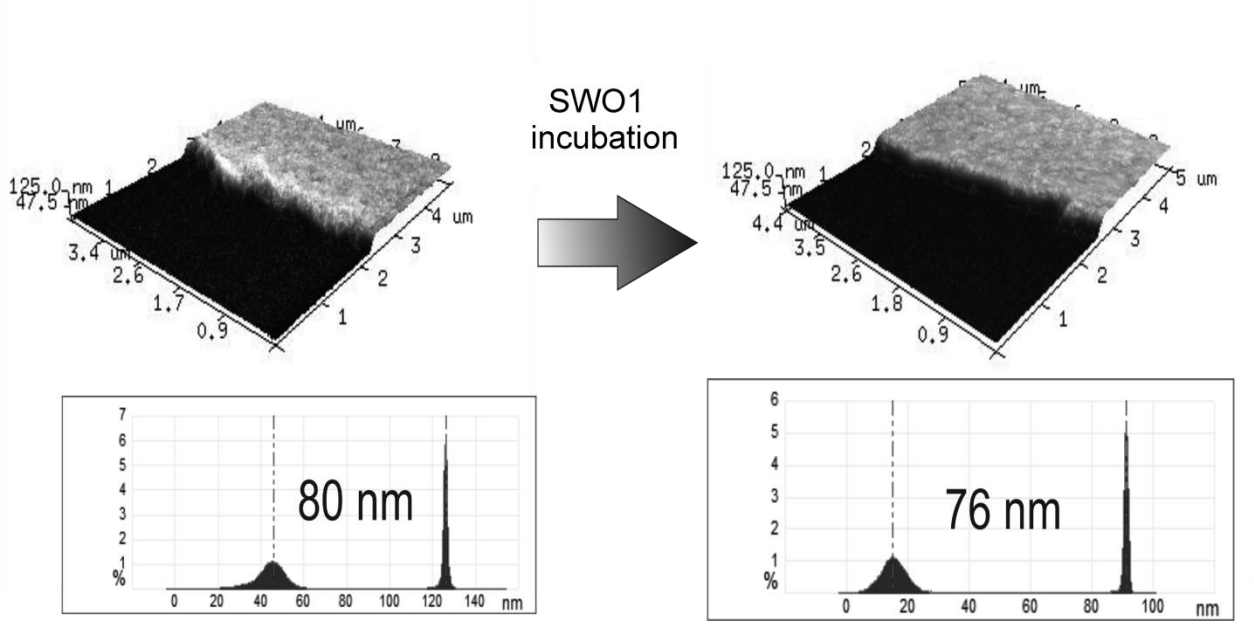

Figure 10: Comparison of height profiles of SWO1-treated and untreated C2. The three-dimensional height profile of untreated C2 (top left) was evaluated and compared to SWO1-treated C2 (top right, 0.4 µM SWO1 for 24 h), resulting in their specific height distributions (bottom left and right).

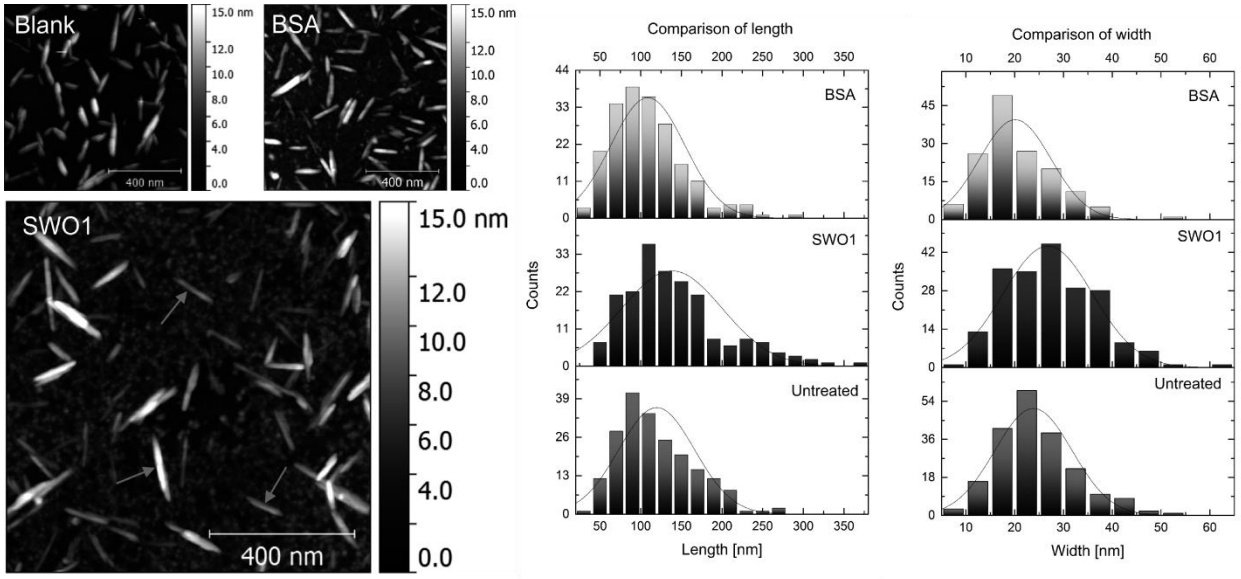

Figure 11: Comparison of length and width of SWO1-treated, BSA-treated and untreated NCC. Left: Typical NCC structures indicated by grey arrows. Middle: Comparison of length-distribution of SWO1-, BSA- and untreated NCC. Right: Comparison of width-distribution of the same.

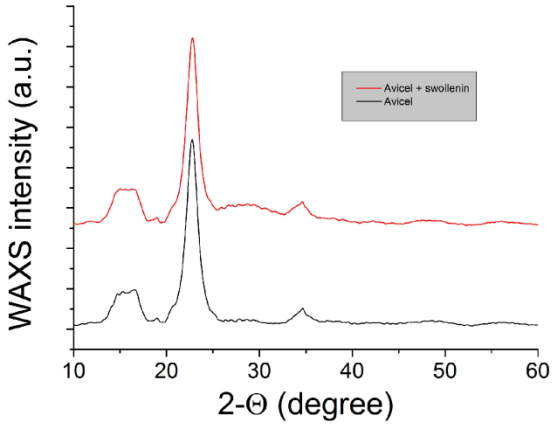

Figure 12 Comparison of WAXS profile of SWO1-treated and untreated Avicel.

To verify the results of the AFM measurement a WAXS analysis of SWO1-treated and untreated Avicel was carried out. In case SWO1 would have an expansin-like effect on the pure cellulosic Avicel, the crystallinity of Avicel would have been affected similarly to the gradual shift of Avicel turned amorphous cellulose described in Ganner et al. 2014 [67]. Nevertheless, in accord with the AFM-results, no effect on the crystallinity was detectable after 72 h of SWO1 incubation (Fig 12).

Determination of synergism effects of SWO1 with SVG on dried grass

Measurements on dried *Dactylis glomerata* grass turned out to be difficult, because of the heterogeneity and resistance of the material. We could determine a marginal synergism effect of SWO1 with SVG after 164 h, measured in duplicates (Fig 13). These results correspond with a synergism effect of 1.66 that could be determined for undefined grass after 72 h (Data not shown). Despite the high standard deviations we support the model of SWO1 as a root colonization factor, which cannot act on pure cellulosic substrates, but has an effect on a macroscopic scale perhaps on plant cell walls [68,69]. This theory is supported by a study, where SWO1 was silenced in a *Trichoderma aperellum*

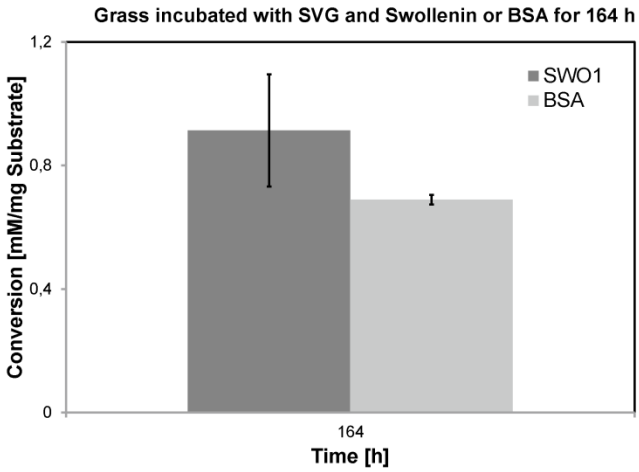

Figure 13: Amount of released sugar from 1mg/ml grass after 164 h of incubation with 1µM SWO1 and 2 µg SVG per mg grass.

strain, by that restraining its growth significantly. Additionally, the same report stated an increasing growth when overexpressing SWO1 [68].

Conclusion

In this study the native form of SWO1 expressed by a genetically engineered *T. reesei* was used for the first time and verified with different methods like circular dichroism, affinity-assays and SDS-PAGE. Since SWO1 did not show any cellulase-like hydrolytic activity, it can be ruled out that the isolated product was contaminated with cellobiohydrolases (CBH) or endoglucanases (EG). Furthermore, the binding affinity of SWO1 to Avicel is comparable to findings in the literature [51] and to other CBD I comprising proteins [46,61]. Moreover, it exhibits affinity for lignin and an order of magnitude higher affinity for xylan. These findings correspond well with the proposed function of SWO1 as a lignocellulose-active protein [49,51]. SWO1 also has the function to release a minor portion of reducing sugars from cellulosic substrates and β-glucan. Surprisingly, but conforming with the literature [64], SWO1 has the ability to effectively degrade cellotetraose. The mechanism is not yet determined; so far Andberg et al. (2015) [64] has suggested that SWO1 has an endoglucanase-function of cutting within cellulose-chains, however, subsequently then releasing cellobiose in a cellobiohydrolase manner.

Moreover, our data demonstrate that *T. reesei* SWO1 neither imposes amorphogenesis nor any other kind of structural alteration on pure cellulosic substrates. These findings were confirmed visually by AFM-measurements and additionally by WAXS. Correspondingly, no synergism with fungal cellulases on pure cellulosic substrates was detectable, though this finding stands in contrast to results found in the literature [51]. Results, indicating that SWO1 might synergize with fungal cellulases on non-treated natural substrates, e.g. grass, lead us to the conclusion that the function of SWO1 is not targeted at pure cellulosic substrates, but rather reveals its function

when exposed to natural substrates with a specific macroscopic varied structure confirming with root-colonization concepts in the literature [68,69].

Acknowledgements

First and foremost I want to express my sincere gratitude to Univ.-Prof. Dipl.-Ing. Dr. techn. Bernd Nidetzky, Dipl.-Ing. Dr. techn. Harald Plank, Dipl.-Ing. Manuel Eibinger and Dipl.-Ing. Thomas Ganner from Graz University of Technology for their kind encouragement and supervision. Also, I want to thank Dipl.-Ing. Jürgen Sattelkow from Graz University of Technology for his good cooperation in the AFM-measurements and Dr. rer. nat. Bernhard Seiboth and his group from Vienna University of Technology for providing us with *T. reesei* supernatant. From University of Graz I want to thank Dipl.-Biol. Dr. rer. nat. habil. Christian Berg for different kinds of grass sorts provided and Christian Fercher, MSc, for his guidance in the circular dichroism measurement.

References

1. Solomon BD, Barnes JR, Halvorsen KE. Grain and cellulosic ethanol: History, economics, and energy policy. Biomass and Bioenergy. 2007;31: 416–425. doi:10.1016/j.biombioe.2007.01.023

2. Lynd LRL, Weimer PPJ, van Zyl W, Pretorius IS, Zyl WH Van. Microbial cellulose utilization: fundamentals and biotechnology. Microbiol Mol Biol Rev. 2002;66: 506–577. doi:10.1128/MMBR.66.3.506

3. Himmel ME, Ding S-Y, Johnson DK, Adney WS, Nimlos MR, Brady JW, et al. Biomass recalcitrance: engineering plants and enzymes for biofuels production. Science. 2007;315: 804–7. doi:10.1126/science.1137016

4. Cosgrove DJ. New genes and new biological roles for expansins. Curr Opin Plant Biol. 2000;3: 73–78.

5. O´Dwyer JP. Developing a fundamental understanding of biomass structural features responsible for enzymatic digestibility. 2005. p. 313.

6. Zhao X, Zhang L, Liu D. Biomass recalcitrance . Part I : the chemical compositions and physical structures affecting the enzymatic hydrolysis of lignocellulose. Biofuels, Bioprod Biorefining. 2012;6: 465–482. doi:10.1002/bbb

7. Karhumaa K, Hahn-Hägerdal B, Gorwa-Grauslund M-F. Investigation of limiting metabolic steps in the utilization of xylose by recombinant Saccharomyces cerevisiae using metabolic engineering. Yeast. 2005;22: 359–68. doi:10.1002/yea.1216

8. Antoni D, Zverlov V V, Schwarz WH. Biofuels from microbes. Appl Microbiol Biotechnol. 2007;77: 23–35. doi:10.1007/s00253-007-1163-x

9. Ha S, Galazka JM, Rin S, Choi J, Yang X, Seo J. Engineered Saccharomyces cerevisiae capable of simultaneous cellobiose and xylose fermentation. Proc Natl Acad Sci U S A. 2011;108: 504–509. doi:10.1073/pnas.1010456108/-/DCSupplemental.www.pnas.org/cgi/doi/10.1073/pnas.1010456108

10. Lora JH, Glasser WG. Recent Industrial Applications of Lignin : A Sustainable Alternative to Nonrenewable Materials. J Polym Environ. 2002;10: 39–48.

11. Hahn-Hägerdal B, Galbe M, Gorwa-Grauslund MF, Lidén G, Zacchi G. Bio-ethanol--the fuel of tomorrow from the residues of today. Trends Biotechnol. 2006;24: 549–56. doi:10.1016/j.tibtech.2006.10.004

12. Naik SN, Goud V V., Rout PK, Dalai AK. Production of first and second generation biofuels: A comprehensive review. Renew Sustain Energy Rev. 2010;14: 578–597. doi:10.1016/j.rser.2009.10.003

13. Sims REH, Mabee W, Saddler JN, Taylor M. An overview of second generation biofuel technologies. Bioresour Technol. Elsevier Ltd; 2010;101: 1570–80. doi:10.1016/j.biortech.2009.11.046

14. Alvira P, Tomás-Pejó E, Ballesteros M, Negro MJ. Pretreatment technologies for an efficient bioethanol production process based on enzymatic hydrolysis: A review. Bioresour Technol. Elsevier Ltd; 2010;101: 4851–61. doi:10.1016/j.biortech.2009.11.093

15. Da Costa Sousa L, Chundawat SPS, Balan V, Dale BE. “Cradle-to-grave” assessment of existing lignocellulose pretreatment technologies. Curr Opin Biotechnol. 2009;20: 339–47. doi:10.1016/j.copbio.2009.05.003

16. Hendriks a TWM, Zeeman G. Pretreatments to enhance the digestibility of lignocellulosic biomass. Bioresour Technol. 2009;100: 10–8. doi:10.1016/j.biortech.2008.05.027

17. Kumar P, Barrett DM, Delwiche MJ, Stroeve P. Methods for Pretreatment of Lignocellulosic Biomass for Efficient Hydrolysis and Biofuel Production. Ind Eng Chem Res. 2009;48: 3713–3729. doi:10.1021/ie801542g

18. Lee SH, Doherty T V, Linhardt RJ, Dordick JS. Ionic liquid-mediated selective extraction of lignin from wood leading to enhanced enzymatic cellulose hydrolysis. Biotechnol Bioeng. 2009;102: 1368–76. doi:10.1002/bit.22179

19. Mosier N, Wyman C, Dale B, Elander R, Lee YY, Holtzapple M, et al. Features of promising technologies for pretreatment of lignocellulosic biomass. Bioresour Technol. 2005;96: 673–86. doi:10.1016/j.biortech.2004.06.025

20. Pérez J, Muñoz-Dorado J, de la Rubia T, Martínez J. Biodegradation and biological treatments of cellulose, hemicellulose and lignin: an overview. Int Microbiol. 2002;5: 53–63. doi:10.1007/s10123-002-0062-3

21. Taherzadeh MJ, Karimi K. Pretreatment of lignocellulosic wastes to improve ethanol and biogas production: a review. [Internet]. International journal of molecular sciences. 2008. pp. 1621–51. doi:10.3390/ijms9091621

22. Wyman CE, Dale BE, Elander RT, Holtzapple M, Ladisch MR, Lee YY. Coordinated development of leading biomass pretreatment technologies. Bioresour Technol. 2005;96: 1959–66. doi:10.1016/j.biortech.2005.01.010

23. Wang Y, Tang R, Tao J, Gao G, Wang X, Mu Y, et al. Quantitative investigation of non-hydrolytic disruptive activity on crystalline cellulose and application to recombinant swollenin. Appl Microbiol Biotechnol. 2011;91: 1353–63. doi:10.1007/s00253-011-3421-1

24. Yang B, Wyman CE. Pretreatment : the key to unlocking low-cost cellulosic ethanol. 2008; 26–40. doi:10.1002/bbb

25. Zhao H, Jones CL, Baker G a, Xia S, Olubajo O, Person VN. Regenerating cellulose from ionic liquids for an accelerated enzymatic hydrolysis. J Biotechnol. 2009;139: 47–54. doi:10.1016/j.jbiotec.2008.08.009

26. Zheng Y, Pan Z, Zhang R. Overview of biomass pretreatment for cellulosic ethanol production. Int J Agric Biol Eng. 2009;2: 51–68. doi:10.3965/j.issn.1934-6344.2009.03.051-068

27. Zhu JY, Pan X, Zalesny RS. Pretreatment of woody biomass for biofuel production: energy efficiency, technologies, and recalcitrance. Appl Microbiol Biotechnol. 2010;87: 847–57. doi:10.1007/s00253-010-2654-8

28. Grous WR, Converse AO, Grethlein HE. Effect of steam explosion pretreatment on pore size and enzymatic hydrolysis of poplar. Enzyme Microb Technol. 1986;8: 274–280.

29. Chundawat SPS, Bellesia G, Uppugundla N, Sousa C, Gao D, Cheh AM, et al. Restructuring the Crystalline Cellulose Hydrogen Bond Network Enhances Its Depolymerization Rate. J Am Chem Soc. 2011;133: 11163–11174.

30. Chang VS, Holtzapple MT. Fundamental factors affecting biomass enzymatic reactivity. Appl Biochem Biotechnol. 2000;84-86: 5–37.

31. Béguin P, Aubert J-P. Crystalline region. FEMS Microbiol Rev. 1994;13: 25–58.

32. Jørgensen H, Kristensen JB, Felby C. Enzymatic conversion of lignocellulose into fermentable sugars : challenges and opportunities. Biofuels, Bioprod Biorefining. 2007;1: 119–134. doi:10.1002/bbb

33. Mohnen D, Bar-Peled M, Somerville C. Cell Wall Polysaccharide Synthesis. 2008. pp. 94–187.

34. Shen T, Gnanakaran S. The stability of cellulose: a statistical perspective from a coarse-grained model of hydrogen-bond networks. Biophys J. Biophysical Society; 2009;96: 3032–40. doi:10.1016/j.bpj.2008.12.3953

35. Zhu JY, Wang GS, Pan XJ, Gleisner R. Specific surface to evaluate the efficiencies of milling and pretreatment of wood for enzymatic saccharification. Chem Eng Sci. 2009;64: 474–485. doi:10.1016/j.ces.2008.09.026

36. Doi RH, Kosugi A. Cellulosomes: plant-cell-wall-degrading enzyme complexes. Nat Rev Microbiol. 2004;2: 541–51. doi:10.1038/nrmicro925

37. Fontes CMG a, Gilbert HJ. Cellulosomes: highly efficient nanomachines designed to deconstruct plant cell wall complex carbohydrates. Annu Rev Biochem. 2010;79: 655–81. doi:10.1146/annurev-biochem-091208-085603

38. Nidetzky B, Steiner W, Hayn M, Claeyssens M. Cellulose hydrolysis by the cellulases from Trichoderma reesei: a new model for synergistic interaction. Biochem J. 1994;298 Pt 3: 705–10. Available: http://www.pubmedcentral.nih.gov/articlerender.fcgi?artid=1137917&tool=pmcentrez&rendertype=abstract

39. Zhang Y-HP, Lynd LR. Toward an aggregated understanding of enzymatic hydrolysis of cellulose: noncomplexed cellulase systems. Biotechnol Bioeng. 2004;88: 797–824. doi:10.1002/bit.20282

40. Coughlan MP. The Properties of Fungal and Bacterial Cellulases with Comment on their Production and Application. Biotechnol Genet Eng Rev. 1985;3: 39–110. doi:10.1080/02648725.1985.10647809

41. Din N, Gilkes NR, Tekant B, Miller RC, Warren AJ, Kilburn DG. Non-hydrolytic disruption of cellulose fibres by the binding domain of a bacterial cellulase. Nature. 1991;9: 1096–1099.

42. Arantes V, Saddler JN. Access to cellulose limits the efficiency of enzymatic hydrolysis : the role of amorphogenesis. Biotechnol Biofuels. 2010;3: 1–11.

43. Lin H, Shen Q, Zhan J-M, Wang Q, Zhao Y-H. Evaluation of bacterial expansin EXLX1 as a cellulase synergist for the saccharification of lignocellulosic Agro-industrial wastes. PLoS One. 2013;8: e75022. doi:10.1371/journal.pone.0075022

44. Din N, Damude HG, Gilkes NR, Miller RC, Warren RAJ, Kilburn DG. C1-CX , revisited : Intramolecular synergism in a cellulase. Proc Natl Acad Sci U S A. 1994;91: 11383–11387.

45. Liu X, Ma Y, Zhang M. Research advances in expansins and expansion-like proteins involved in lignocellulose degradation. Biotechnol Lett. Springer Netherlands; 2015; doi:10.1007/s10529-015-1842-0

46. Bunterngsook B, Eurwilaichitr L, Thamchaipenet A, Champreda V. Binding characteristics and synergistic effects of bacterial expansins on cellulosic and hemicellulosic substrates. Bioresour Technol. Elsevier Ltd; 2015;176: 129–35. doi:10.1016/j.biortech.2014.11.042

47. Kim ES, Lee HJ, Bang W-G, Choi I-G, Kim KH. Functional characterization of a bacterial expansin from Bacillus subtilis for enhanced enzymatic hydrolysis of cellulose. Biotechnol Bioeng. 2009;102: 1342–53. doi:10.1002/bit.22193

48. Chen X, Ishida N, Todaka N, Nakamura R, Maruyama J, Takahashi H, et al. Promotion of efficient Saccharification of crystalline cellulose by Aspergillus fumigatus Swo1. Appl Environ Microbiol. 2010;76: 2556–61. doi:10.1128/AEM.02499-09

49. Saloheimo M, Paloheimo M, Hakola S, Pere J, Swanson B, Nyyssönen E, et al. Swollenin, a Trichoderma reesei protein with sequence similarity to the plant expansins, exhibits disruption activity on cellulosic materials. Eur J Biochem. 2002;269: 4202–4211. doi:10.1046/j.1432-1033.2002.03095.x

50. Verma D, Jin S, Kanagaraj A, Singh ND, Daniel J, Kolattukudy PE, et al. Expression of fungal cutinase and swollenin in tobacco chloroplasts reveals novel enzyme functions and/or substrates. PLoS One. 2013;8: e57187. doi:10.1371/journal.pone.0057187

51. Jäger G, Girfoglio M, Dollo F, Rinaldi R, Bongard H, Commandeur U, et al. How recombinant swollenin from Kluyveromyces lactis affects cellulosic substrates and accelerates their hydrolysis. Biotechnol Biofuels. 2011;4: 33. doi:10.1186/1754-6834-4-33

52. Gourlay K, Hu J, Arantes V, Andberg M, Saloheimo M, Penttilä M, et al. Swollenin aids in the amorphogenesis step during the enzymatic hydrolysis of pretreated biomass. Bioresour Technol. Elsevier Ltd; 2013;142: 498–503. doi:10.1016/j.biortech.2013.05.053

53. Wang W, Liu C, Ma Y, Liu X, Zhang K, Zhang M. Improved production of two expansin-like proteins in Pichia pastoris and investigation of their functional properties. Biochem Eng J. Elsevier B.V.; 2014;84: 16–27. doi:10.1016/j.bej.2013.12.018

54. Medve J, Lee D, Tjerneld F. Ion-exchange chromatographic purification and quantitative analysis of Trichoderma reesei cellulases cellobiohydrolase I , II and endoglucanase II by fast protein liquid chromatography. J Chromatogr A. 1998;808: 153–165.

55. Wildberger P, Aish G a., Jakeman DL, Brecker L, Nidetzky B. Interplay of catalytic subsite residues in the positioning of α-d-glucose 1-phosphate in sucrose phosphorylase. Biochem Biophys Reports. Elsevier; 2015;2: 36–44. doi:10.1016/j.bbrep.2015.04.001

56. Habibi Y, Lucia LA, Rojas OJ. Cellulose Nanocrystals : Chemistry , Self-Assembly , and Applications. Am Chem Soc. 2009; A–V.

57. Eibinger M, Bubner P, Ganner T, Plank H, Nidetzky B. Surface structural dynamics of enzymatic cellulose degradation, revealed by combined kinetic and atomic force microscopy studies. FEBS J. 2014;281: 275–90. doi:10.1111/febs.12594

58. O'Sullivan AC. Cellulose : the structure slowly unravels. Cellulose. 1997;4: 173–207.

59. Xiao Z, Storms R, Tsang A. Microplate-based filter paper assay to measure total cellulase activity. Biotechnol Bioeng. 2004;88: 832–7. doi:10.1002/bit.20286

60. Peterson R, Nevalainen H. Trichoderma reesei RUT-C30--thirty years of strain improvement. Microbiology. 2012;158: 58–68. doi:10.1099/mic.0.054031-0

61. Guo J, Catchmark J. Binding specificity and thermodynamics of cellulose-binding modules from Trichoderma reesei Cel7A and Cel6A. Biomacromolecules. 2013;14: 1268–1277. Available: http://pubs.acs.org/doi/abs/10.1021/bm300810t

62. Teleman A, Larsson PT, Iversen T. On the accessibility and structure of xylan in birch kraft pulp. Cellulose. 2001;8: 209–215.

63. Jeoh T, Ishizawa CI, Davis MF, Himmel ME, Adney WS, Johnson DK. Cellulase Digestibility of Pretreated Biomass Is Limited by Cellulose Accessibility. Biotechnol Bioeng. 2007;98: 112–122. doi:10.1002/bit

64. Andberg M, Penttilä M, Saloheimo M. Swollenin from Trichoderma reesei exhibits hydrolytic activity against cellulosic substrates with features of both endoglucanases and cellobiohydrolases. Bioresour Technol. Elsevier Ltd; 2015;181: 105–13. doi:10.1016/j.biortech.2015.01.024

65. Kafle K, Xi X, Lee CM, Tittmann BR, Cosgrove DJ, Park YB, et al. Cellulose microfibril orientation in onion (Allium cepa L.) epidermis studied by atomic force microscopy (AFM) and vibrational sum frequency generation (SFG) spectroscopy. Cellulose. 2013;21: 1075–1086. doi:10.1007/s10570-013-0121-2

66. Ganner T, Bubner P, Eibinger M, Mayrhofer C, Plank H, Nidetzky B. Dissecting and reconstructing synergism: in situ visualization of cooperativity among cellulases. J Biol Chem. 2012;287: 43215–43222. doi:10.1074/jbc.M112.419952

67. Ganner T, Aschl T, Eibinger M, Bubner P, Meingast A, Chernev B, et al. Tunable mixed amorphous–crystalline cellulose substrates (MACS) for dynamic degradation studies by atomic force microscopy in liquid environments. Cellulose. 2014;21: 3927–3939. doi:10.1007/s10570-014-0419-8

68. Brotman Y, Briff E, Viterbo A, Chet I. Role of swollenin, an expansin-like protein from Trichoderma, in plant root colonization. Plant Physiol. 2008;147: 779–89. doi:10.1104/pp.108.116293

69. Gaulin E, Dramé N, Lafitte C, Torto-Alalibo T, Martinez Y, Amaline-Toregrosa C, et al. Cellulose Binding Domains of a Phytophthora Cell Wall Protein Are Novel Pathogen-Associated Molecular Patterns. Plant Cell. 2006;18: 1766–1777. doi:10.1105/tpc.105.038687.1

Appendix 1: Supplementary Information about SWO1

Short declaration

In this section of my master thesis are further ideas and experiments contributing to the knowledge of SWO1 that have not been incorporated into the paper draft. They either include information on aspects of SWO1 that did not quite well fit into the context of the paper or experiments that showed low quality-images, high standard abbreviations or could not be reproduced. Nevertheless, some data might be of value for further investigations.

Materials and methods

SWO1 purification

SWO1 was isolated from *T. reesei* RUT C-30 supernatant employing an ion-exchange chromatography. *T. reesei* RUT C-30 supernatant was first filtrated with a 0.2 µm polyethersulfone filter (Sartorius) and loaded onto a Duoflow chromatography system with an Auto-Injection Valve AVR7-3 and a Model 2128 Fraction Collection (BIO-RAD) employing a Q-column (Resource). 20 mM TEA at pH 7.0 was used as running buffer and 20 mM TEA and 1 M NaCl at pH 7.0 was used as the elution buffer. The concentration of elution buffer was increased gradually to be able to isolate SWO1 in a relatively pure form. To identify the SWO1 peak, a minor portion of *T. reesei* supernatant was incubated with Avicel to remove SWO1 due to its binding affinity to cellulose. The SWO1-free supernatant was loaded on the Duoflow system and showed a chromatogram, which missed a distinct peak in comparison to SWO1-containing supernatant. With that knowledge SWO1 could be isolated and was subjected to further processing: the buffer was adjusted with reaction buffer and SWO1 was concentrated by centrifugation in spin filter columns at 5000 rpm and 4 °C.

The protein concentration was determined by UV-absorption on a Nanodrop system with a calculated absorption of 1.704 for 1 g/l (ProtParam) at 280 nm and the purification was evaluated with SDS-PAGE, using a protein marker for the evaluation of proteins with a molecular weight of 10-200 kDa.

Modelling with RaptorX

In addition to the modelling carried out with Phyre2, the sequence of SWO1 was uploaded to RaptorX and a 3D-model was calculated.

Adsorption experiments

Supplementary to the binding experiments with Avicel, birch wood xylan and lignin, the affinity of SWO1 was determined for autoclaved wheat straw and, as a function of time, for Avicel and phosphoric acid swollen cellulose (PASC).

Autoclaved wheat straw

Autoclaved wheat straw was friendly provided by Dipl.-Ing. B.Sc. BSc Vera Novy [70,71]. 1 mg/ml of autoclaved wheat straw was incubated with 0.2, 0.4, 0.7, 1 and 2 µM of SWO1 in 1.5 ml tubes (Sarstedt) in reaction buffer with a working volume of 50 µl on a thermomixer (Eppendorf) at 25 °C and 500 rpm. After 2 h the samples were centrifuged for 5 min at 13.000 rpm and 4 °C and the supernatant was transferred into new 1.5 ml tubes. The experiments were carried out in duplicates and the protein concentration of the supernatant was determined by Roti-Nanoquant (ROTH) (xylan, lignin) following the instructions of the manufacturer and with a CBH1 standard in the range of 20-200 µg/ml.

PASC and Avicel

PASC was produced accordingly to the protocol by Walseth et al. (1952) [72]. 3 mg/ml of PASC and 5mg/ml of Avicel were incubated with 0.46 µM of SWO1 in 2 ml tubes (Sarstedt) in reaction buffer with a working volume of 2 ml on a thermomixer (Eppendorf) at 40 °C and 350 rpm.

Samples were taken, when the reaction was started and again after 0, 1, 2, 3, 24, 72 and 96 h. The samples were centrifuged for 1 min at 13.000 rpm and 4 °C to and the supernatant was transferred into new 2 ml tubes. The experiments were carried out in duplicates and the protein concentration of the supernatant was determined by Roti-Nanoquant (ROTH) (xylan, lignin) following the instructions of the manufacturer and with a BSA standard in the range of 0.1-0.8 µM.

In all three experiments the calculation of bound protein the following formula was employed: *Protein added [µM] - Protein in supernatant [µM] – Protein in substrate control [µM] = Bound Protein [µM]*

SWO1 activity measurements

The activity of SWO1 was determined on dried grass (*D. glomerata),* filter paper (Whatman nr. 1), Avicel and onion epidermis under different conditions and utilizing different evaluation methods. Moreover, SWO1 as colonization factor was tested with *E. coli* Origami B (DE3) (Novagen).

D. glomerata grass

1 mg/ml of *D. glomerata* grass was incubated with 0.02 µM of SWO1 or BSA as a reference on a thermomixer at 40 °C and 500 rpm in reaction buffer with a working volume of 1 ml. 100 µl samples were taken after 24 h. The reaction was stopped by adding 100 µl of 100 mM NaOH. The samples were vortexed and centrifuged for 3 min at 13.000 rpm and 4 °C and the supernatants were transferred into new 1.5 reaction tubes. Since we wanted to assess the amount and proportion of all reducing sugars formed, we used a Dionex system with an ED50 electrochemical detector, a GS50 gradient pump and an AS50 autosampler using a Dionex CarboPac PA10 column for monomeric and short-chain sugars. The experiments were done in duplicates and for the calculation of released glucose [%] the formula from sub-chapter *activity measurements on cellulosic substrates* was used and corrected with the dilution factor of NaOH.

Additionally, one experiment was carried out with 1 mg/ml of *D. glomerata* grass incubated with 1 µM of SWO1 or BSA as a reference on a thermomixer at 40 °C and 500 rpm in reaction buffer with a working volume of 1 ml. After several samples and 164 h an image was taken with an Eos 350 D Digital reflex camera (Canon).

Filter paper

The determination of SWO1 activity on filter paper was carried out in duplicates and incubating 1 mg/ml filter paper with 0.4 µM SWO1 in reaction buffer with a working volume of 1 ml on a thermomixer at 40 °C and 500 rpm for 48 h. Subsequently, the evaluation was carried out with a Axioplan light microscopy employing an AxioCam ICc 1 camera and the AxioVision program (ZEISS) at the Institute of Electronmicrscopy and Nanoanalysis. Filter paper incubated in reaction buffer was used as a reference. All further light microscopic investigations were carried out employing the same microscopy system.

Optical evaluation of SWO1 activity on Avicel

1 mg/ml Avicel was incubated with 0.4 µM SWO1 and BSA as a control in reaction buffer with a working volume of 500 µl at 40 °C and 500 rpm on a thermomixer. After 48 h small drops of the mixtures were inspected on microscopic slides with light microscopy. Additionally, one sample of SWO1 with Avicel was supplemented with 1 % TWEEN to see, whether the agglomeration of Avicel fibres was an effect attributable to the water surface tension or to SWO1.

Onion epidermis

A commercial *Allium cepa* onion (Spar) was prepared for light microscopic investigations. Its epidermis was detached and cut into 5x20 mm rectangles. One rectangle per sample was incubated with 0.4 µM SWO1 or BSA in reaction buffer, respectively, directly on a microscopic slide. The slides were put into a petri dish with some drops of reaction buffer for the saturation of air humidity to avoid desiccation, while incubating the samples in a water bath for 24 h. The

measurements were done in duplicates. After the incubation, the results were evaluated with a light microscopy.

SWO1 as a root colonization factor for *E. coli*

This experiment was carried out using spin-cast discs friendly provided by Jürgen Sattelkow from the Institute of Electronmicroscopy and Nanoanalysis. These spin-casts comprise a silica disc layered with cellulose 2, which is an amorphous type of cellulose manufactured by treating cellulose with concentrated sodium hydroxide to either swell or dissolve it, followed by mercerization or precipitation, respectively [58].

These discs were incubated with 0.1 µM SWO1, BSA and only reaction buffer in 5 ml glass beakers with reaction buffer in 2 ml working volume under sterile conditions. The samples were incubated at 40 °C and 110 rpm for 20 h in a water bath. The next day these discs were treated with 125 µl of *E. coli* Origami B (DE3) (Novagen) stock that had been prepared 48 h before and had been incubated with at 30 °C until that time point. The discs were incubated for another hour in a water bath without shaking and were subsequently washed with 10 ml of autoclaved physiologic saline (0.9 % NaCl in ddH_2O). The discs were light microscopically inspected. To repeat this experiment exactly the same conditions were used, however, the light microscopic investigations were carried out with an Infinite Focus microscopy (Alicona) employing to IF-Laboratory Measurement Module 5.1 (Alicona).

Determination of synergism effects with xylanase on birch wood xylan

0.1 µM SWO1 and BSA as a control with 6 ng of a commercial *Trichoderma viride* Xylanase M1 (2300 U/ml, Megazyme) were incubated with 5 mg/ml birch wood xylan in reaction buffer with a working volume of 300 µl at 40 °C and 500 rpm on a thermomixer. After 24 h the reaction was stopped by adding 300 µl of 100 mM NaOH. The samples were vortexed and centrifuged for 3 min at 13.000 rpm and 4 °C and the supernatants were transferred into new 1.5 reaction tubes. For the evaluation of reducing sugars produced a Dionex system with an ED50 electrochemical

detector, a GS50 gradient pump and an AS50 autosampler using a Dionex CarboPac PA10 column for monomeric and short-chain sugars was used. The experiments were done in duplicates and for the calculation of released glucose [%] the formula from sub-chapter *activity measurements on cellulosic substrates* was used and corrected with the dilution factor of NaOH.

Determination of synergism effects of SWO1 with SVG on natural cellulose-comprising substrates

In addition to the synergism-experiment carried out with *D. glomerata* grass, other substrates were also tested. Undefined grass and autoclaved wheat straw were evaluated under different conditions. Furthermore, images of the degradation of *D. glomerata* grass and onion epidermis have been included in the section.

D. glomerata grass

1 mg/ml of *D. glomerata* grass, which was first cut and dried at 80 °C overnight, was incubated with 1 µM of SWO1 or BSA as a reference and 10 µg SVG per mg dried grass on a thermomixer at 40 °C and 500 rpm in reaction buffer with a working volume of 1 ml. After 164 h photos of the degradation were taken with a reflex camera.

Undefined grass

9 mg/ml of undefined grass, which was – in a first trial – picked from outside the institute and dried at 80 °C overnight, were incubated with 0.18 µM of SWO1 and 2 µg SVG per mg dried grass on a thermomixer at 40 °C and 500 rpm in reaction buffer with a working volume of 1 ml. 100 µl samples were taken after 40, 72 and 120 h. The reaction was stopped by adding 100 µl of 100 mM NaOH. The samples were vortexed and centrifuged for 3 min at 13.000 rpm and 4 °C and the supernatants were transferred into new 1.5 reaction tubes. The amount of released glucose in the supernatant was determined by DNS employing the method of Xiao et al. (2004) [59] and using a standard with 4-12 mM glucose. The experiments were done in duplicates and

for the calculation of released glucose [%] the formula from sub-chapter *activity measurements on cellulosic substrates* was used and corrected with the dilution factor of NaOH.

Onion epidermis

A commercial *Allium cepa* onion (Spar) was prepared for light microscopic investigations. Its epidermis was detached and cut into 5x20 mm rectangles. One rectangle per sample was directly incubated with a drop of 0.4 µM SWO1 or BSA, respectively, and 10 µg/ml SVG in reaction buffer on a microscopic slide. The slides were put into a petri dish with some drops of reaction buffer for the saturation of air humidity to avoid desiccation, while incubating the samples in a water bath for 24 h. The measurements were done in duplicates. After the incubation, the results were evaluated with a light microscopy.

Atomic force microscopic measurements

Further measurements on MACS with SWO1 and SVG lead to a broad spectrum of different images. Selected images are shown in this section of my master thesis.

In situ data of substrate surfaces could be obtained by a commercial Dimension 3100 AFM in with a Hybrid scan head, a liquid cell tip holder, a micro-fluid cell in reaction buffer at 40 °C and a Nanoscope IVa controller (Broker AXS). Mixed amorphous-crystalline cellulose model substrate (MACS), analogously prepared to Eibinger et al. (2014) [73], was determined in TappingMode with a FastScanA cantilever (Bruker Nano). Scan rates, set points and drive amplitude were adapted to a gentle tapping interaction of tip and sample. *In situ* AFM imaging of the structural changes upon protein activity was carried out with 0.4 µM SWO1 on MACS. To evaluate the impact of SWO1 on the substrates images of their surface were collected before and after 24 h of incubation with 0.4 µM SWO1. A scan size of 1 x 1 µm² and resolution of 512 x 512 pixels was chosen. The recorded AFM images were processed and analysed using GWYDDION (V2.31).

Results and discussion

SWO1 Purification

First attempts to isolate SWO1 with ion-exchange chromatography showed good results considering the purity of the product (Fig 14). Since we incubated the *T. reesei* RUT C-30 supernatant with Avicel by that removing SWO1 from the solution, we were able to identify the SWO1 peak in the chromatogram (Fig 15, Fig 16). We later turned to affinity chromatography described in the draft for the manuscript, because ion-exchange purification was slow and resulted in a low yield: 0.07 mg in comparison to 0.2 mg per 50 ml of *T. reesei* supernatant. The flow chart in Fig 17 illustrates the two purification methods in detail.

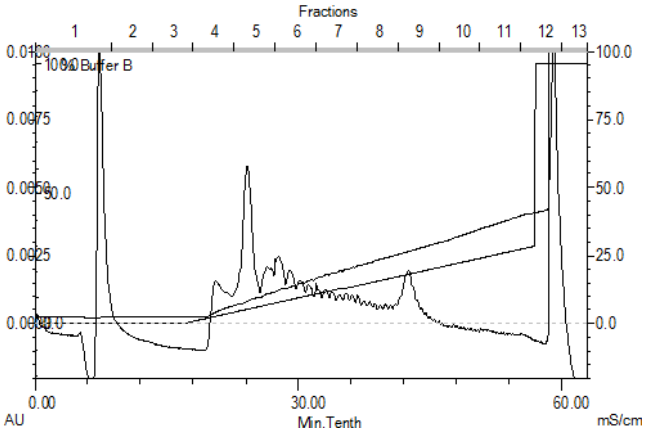

Figure 15 Ion-exchange chromatogram of *T.reessei* RUT C-30 supernatant

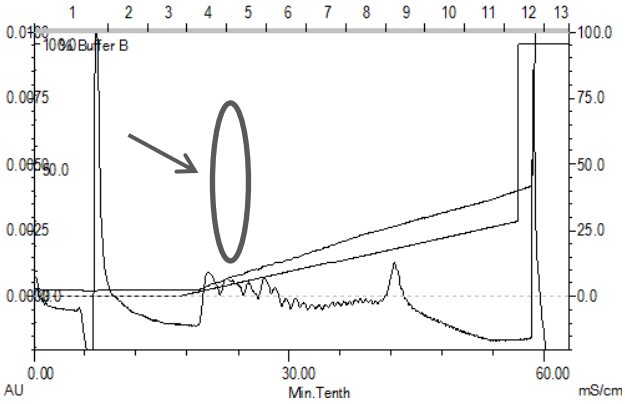

Figure 16 Ion-exchange chromatogram of Avicel-incubated *T.reessei* RUT C-30 supernatant. The arrow indicates the missing peak, by that identifying SWO1

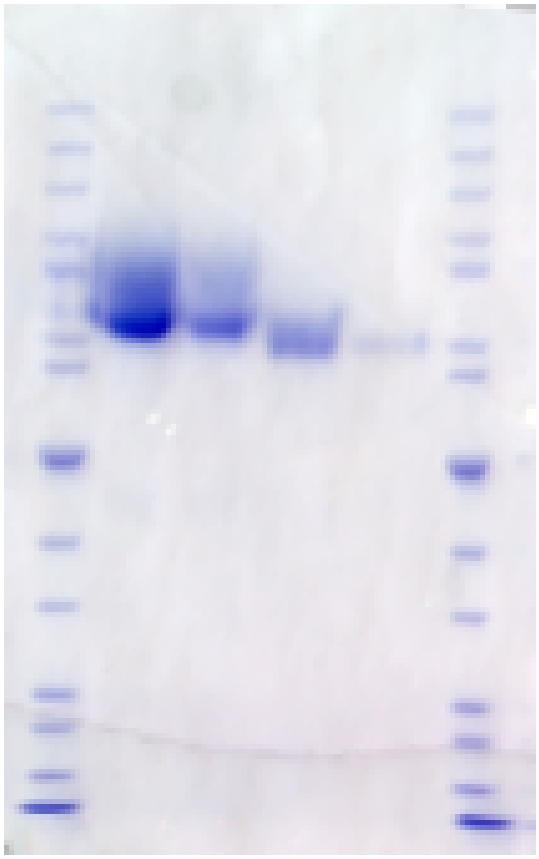

Figure 14 SDS-gel of ion-exchange purified SWO1 fractions

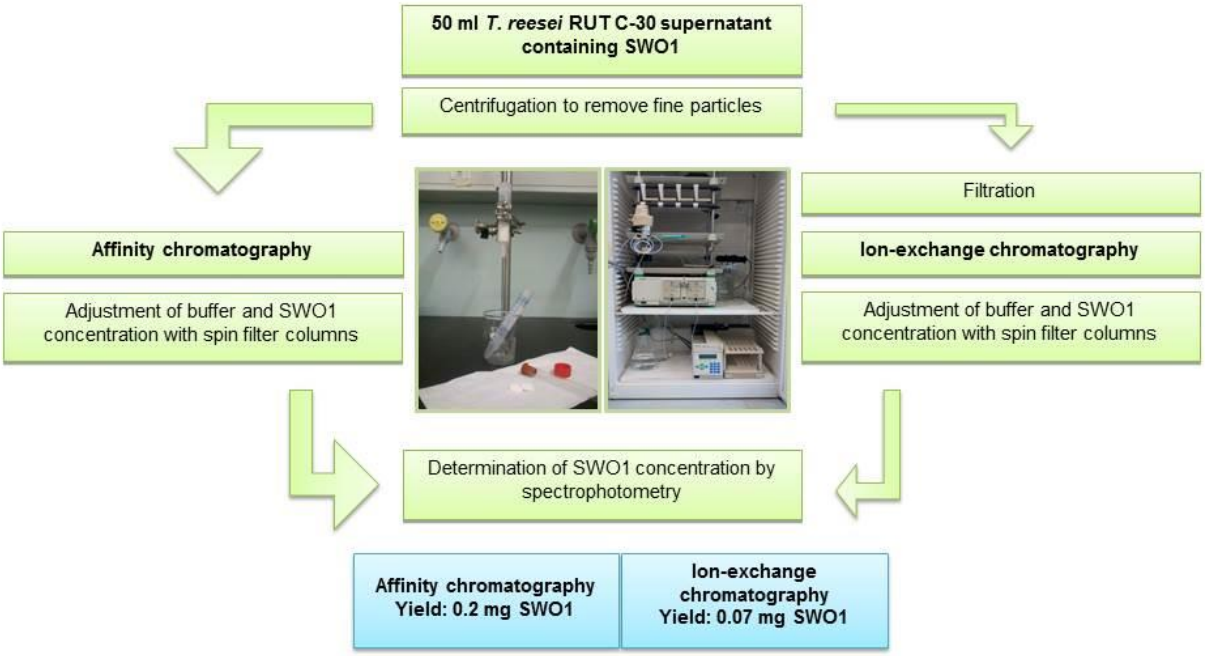

Figure 17 Flow-chart of the two SWO1-purification methods employed. Affinity chromatography in comparison to ion-exchange chromatography.

Modeling with RaptorX

The three-dimensional model of SWO1 calculated by RaptorX (Fig 18) is unstructured and not comparable to other proteins. We propose that this algorithm is not applicable for SWO1.

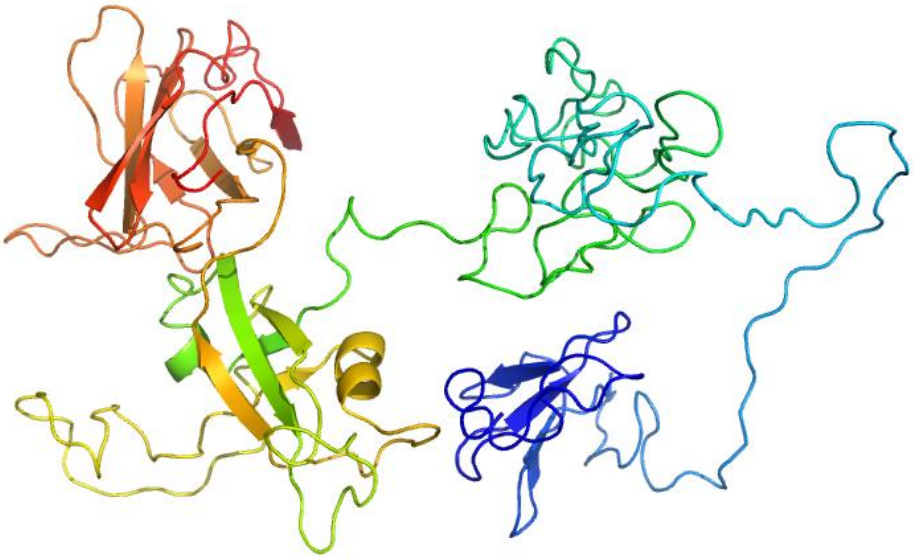

Figure 18 Model of SWO1 calculated by the program RaptorX

Adsorption experiments

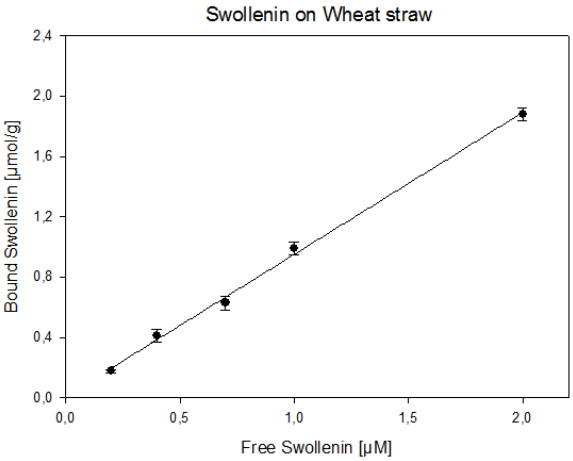

Figure 19 SWO1 binding autoclaved wheat straw

Autoclaved wheat straw

The results show that SWO1 can efficiently bind to autoclaved wheat straw (Fig 19), which is a material that contains many heterologous components, e.g. cellulose, xylan, lignin or cutin. A variety of reports exist that CBDI, therefore SWO1, can bind all of these polymers [2,41,44,69,74–80], which is further emphasized by our results.

PASC and Avicel

The binding of SWO1 to Avicel and PASC was determined over a time range of 96 h (Fig 20). Despite some fluctuation in the beginning of the measurement, the concentration of bound protein to the substrates remains relatively constant.

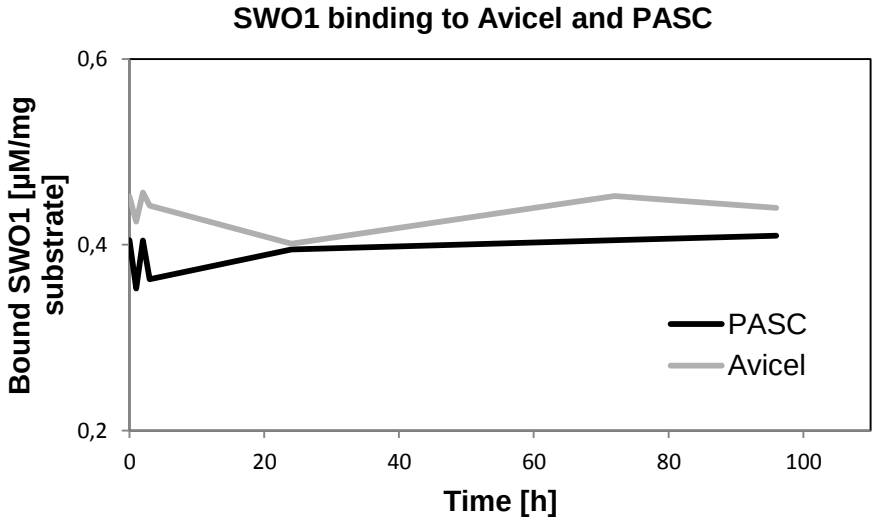

Figure 20 SWO1 binding to Avicel and PASC over a time range of 96 h.

SWO1 activity measurements

D. glomerata grass

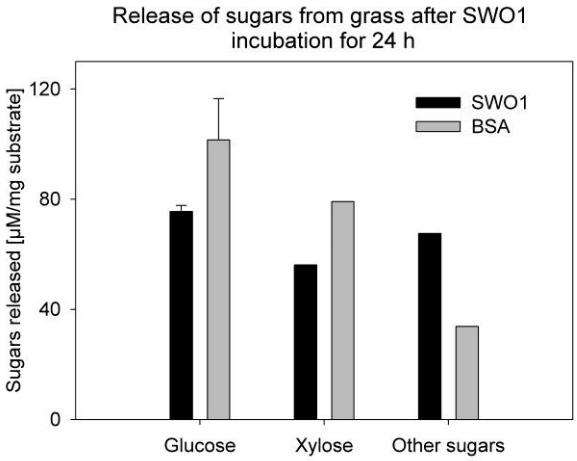

Figure 21: Released sugars from grass after 0.02 µM SWO1 incubation of 5 mg of grass.

Similar to the results of pure cellulosic substrates the incubation of grass with SWO1 results in a minor portion of sugars released (Fig 21). While glucose and xylose are set free in higher amounts by BSA, a greater portion of other monomeric sugars are released by SWO1. Nevertheless, the overall monomeric sugar amount is equal for SWO1- and BSA-treated grass probes.

The preparation of *D. glomerata* grass is shown in Fig 22. Before the SWO1 treatment is was cut and dried at 80 °C. Fig 23 shows an image of SWO1- and BSA- and non-treated grass, which was taken with a reflex camera. With the naked eye all free samples look similar and not in any way swollen or altered. Similar results were obtained when these grass probes were light microscopically inspected (selected images: Fig 24). We could not detect similar swelling of the cell wall as proposed for vesicles of algae [49].

Figure 22 How *D. glomerata* grass was prepared. Cut and dried grass.

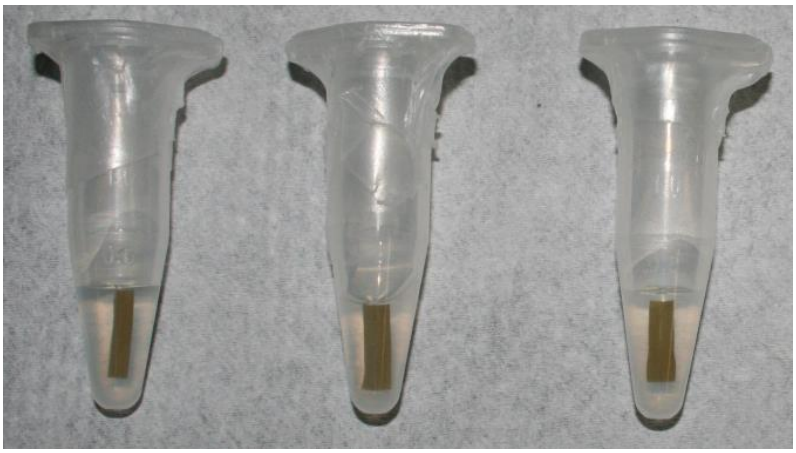

Figure 23 Grass incubated with SWO1 and BSA after 164 h. From left to right: Untreated grass (pure buffer), SWO1- and BSA-treated grass.

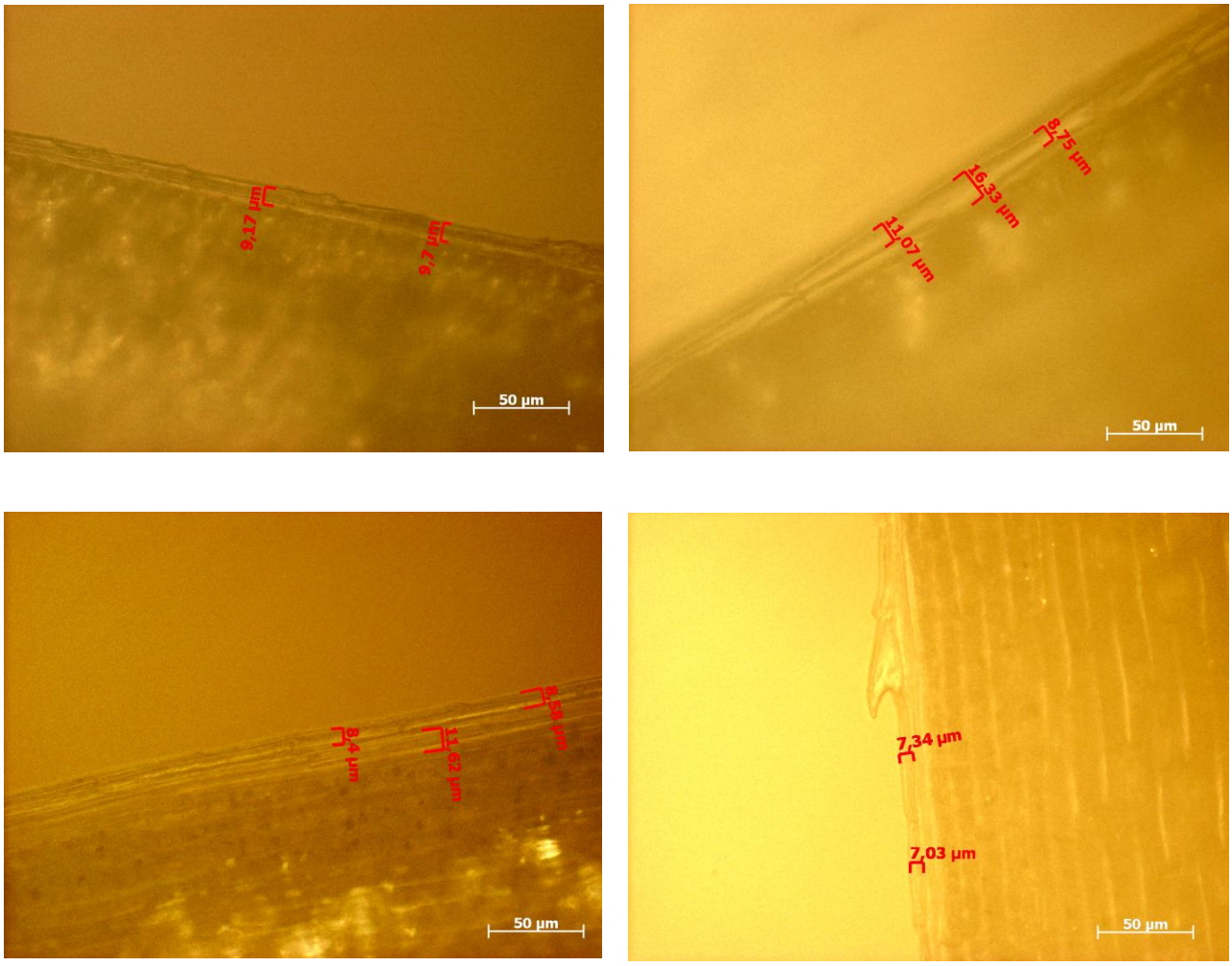

Figure 24 Grass incubated with SWO1 after 164 h. Top left: untreated grass; other images: SWO1-incubated grass. The images also show the dimensions of plant cells.

Filter paper

The light microscopic inspection turned out to be quite difficult due to the density of the paper. Single fibres could hardly be focused (selected images: Fig 25). Nevertheless, we propose images were clear enough to determine that SWO1 does not show an obvious effect on filter paper. This finding is a further attribution to controversial results in the literature. For example, Jäger et al. (2012) [51] reported severe disintegration of filter paper after 48 h of incubation with 5 µM Swollenin.

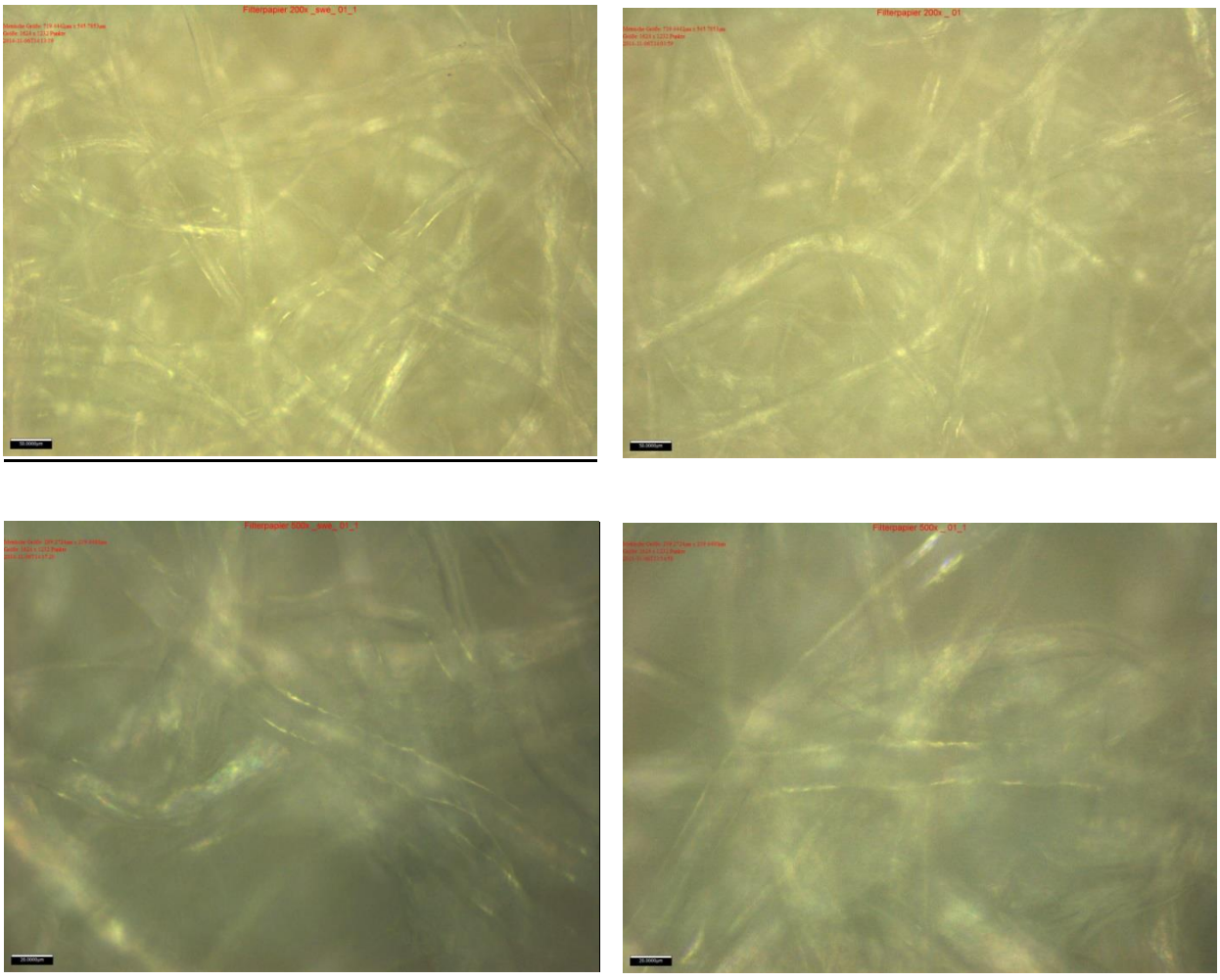

Figure 25 Filter paper incubated for 48 h with 0.4 µM SWO1. Top and bottom left: SWO1 incubated filter paper; Top and bottom right: Untreated filter (buffer) paper; Top: 200-fold magnification; Bottom: 500-fold magnification.

Optical evaluation of SWO1 activity on Avicel

The light microscopic inspection of Avicel also proved to be a difficult task due to their slight movement in the fluid and their radiance. Tough we had presumed that a kind of clumping of the Avicel crystals might be due to an altered surface because of the SWO1 treatment, we later noticed that the clumping resulted from different pressures exerted by the cover slip. Moreover, we could not detect any other alterations of Avicel by either SWO1 or BSA (selected images: Fig 26).

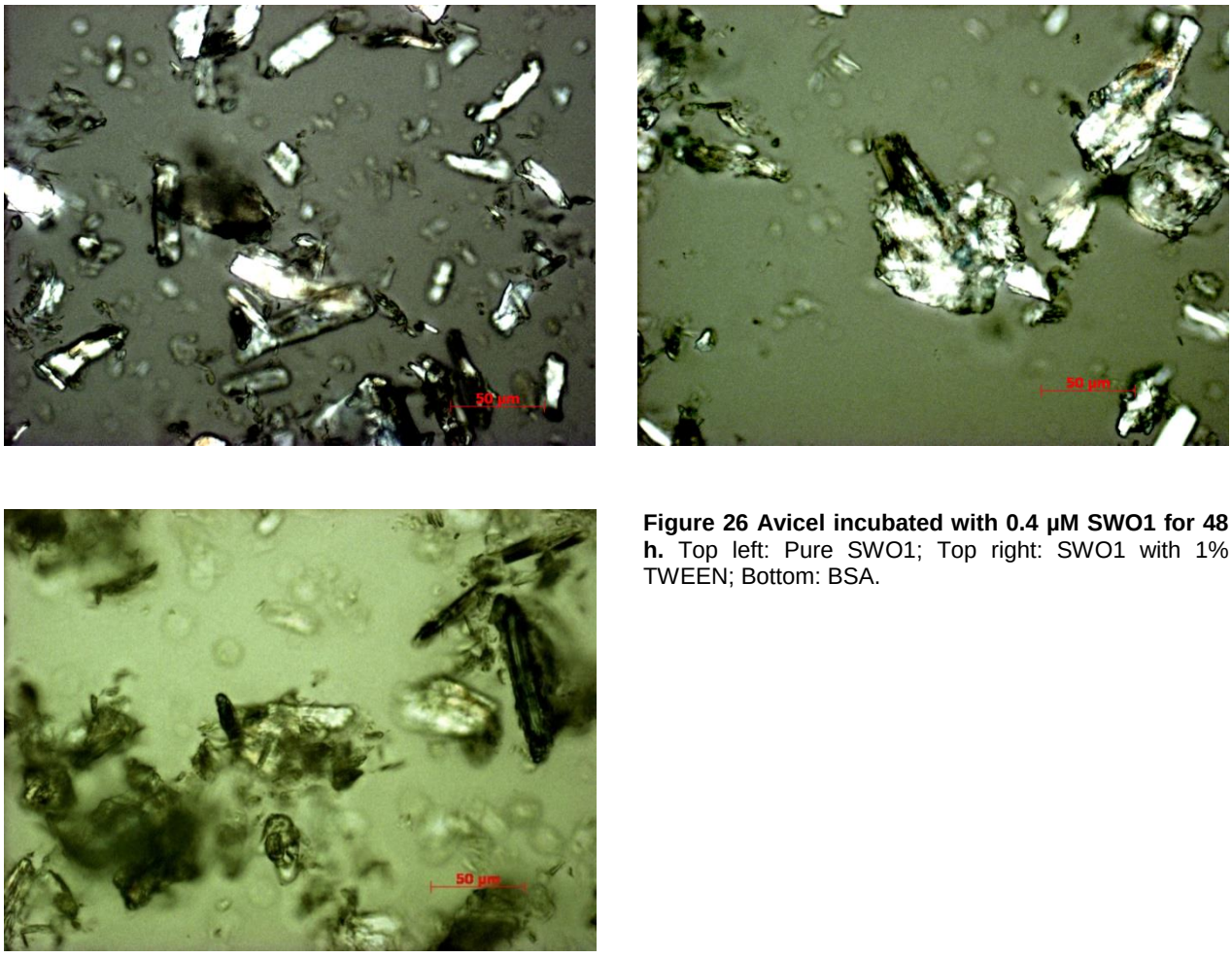

Figure 26 Avicel incubated with 0.4 µM SWO1 for 48 h. Top left: Pure SWO1; Top right: SWO1 with 1% TWEEN; Bottom: BSA.

Onion epidermis

The idea to incubate onion epidermis with SWO1 stems from the determination i) to obtain better images and ii) to find out, whether SWO1 shows an alteration of plant cell walls confirming to the theory as colonization factor [68,69]. Since onion epidermis consists of one layer of cells, the images were far better than in other experiments (Fig 27). Nevertheless, alterations detectable in the image were due to a different focus and all in all, the inspection of a number of images brings us to the conclusion that SWO1 did not show a visible effect on onion epidermis.

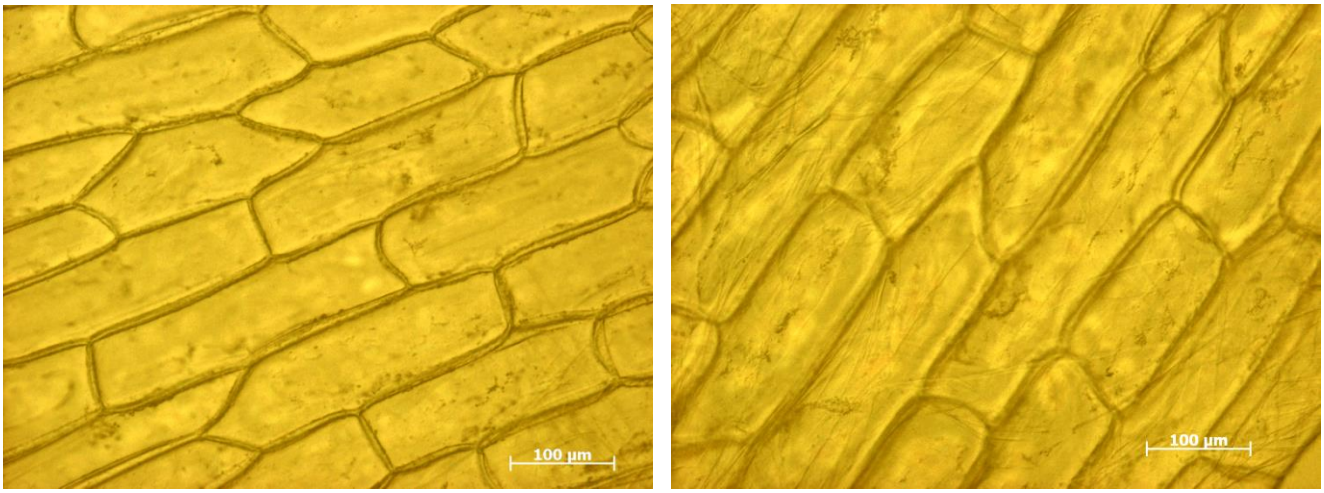

Figure 27 Onion epidermis incubated with 0.4 µM SWO1 for 48 h. Left: SWO1; Right: Buffer.

SWO1 as a root colonization factor for *E.coli*

This experiment was aimed to be a straight forward method to determine, whether the treatment of cellulosic surfaces with SWO1 could result in an enhanced attachment of *E. coli* to the substrate, by that emphasizing the root colonization theory [68]. A first experiment even resulted in an enhanced number of *E. coli* on SWO1-treated in comparison to BSA-treated and untreated amorphous cellulose (Fig 28), but attempts to reproduce the results, failed.

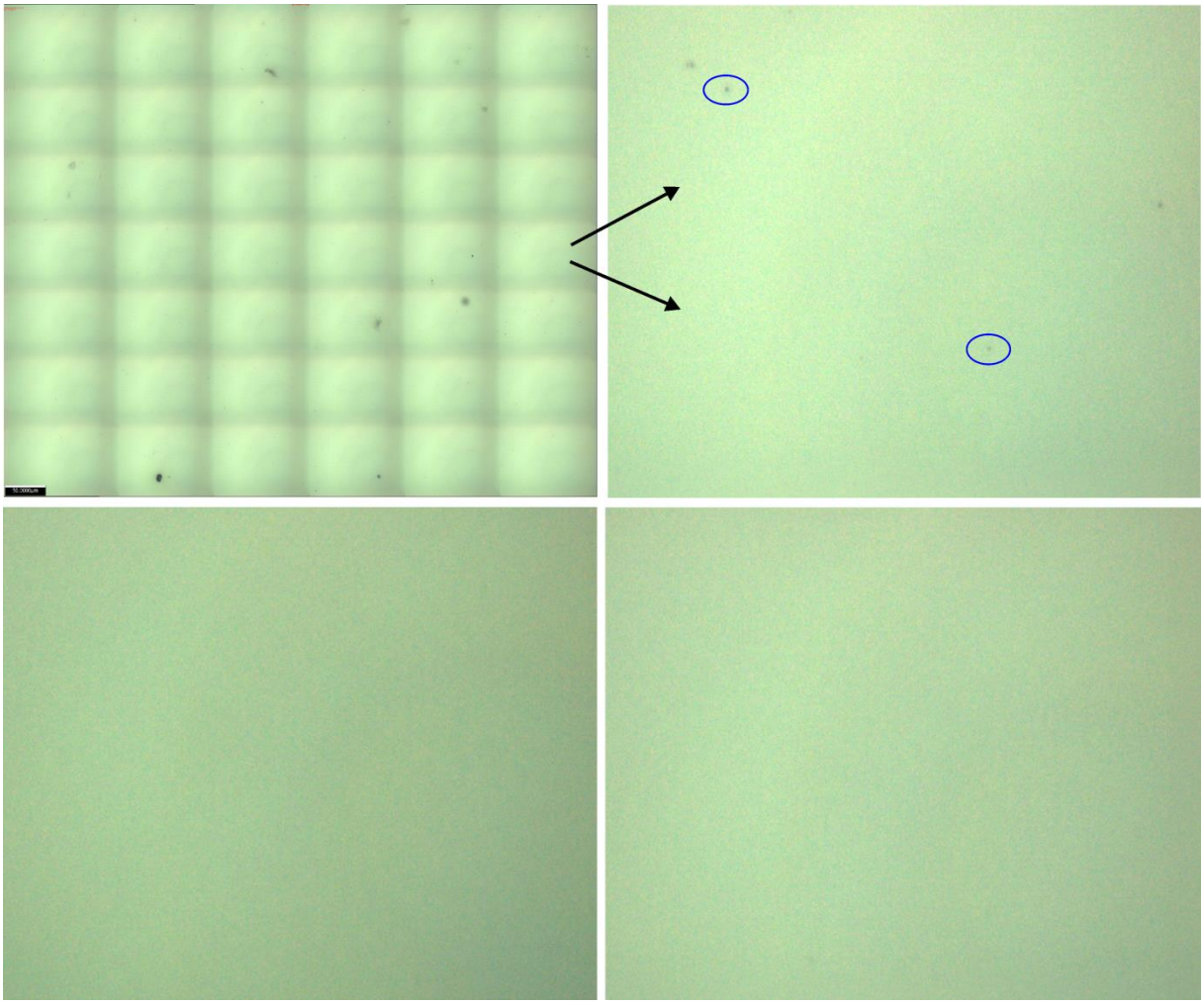

Figure 28 *E. coli* on amorphous substrate. Top left: First rows of images were taken to scan a major part of the cellulosic substrate; Top right: one of the magnified images of SWO1-treated cellulose. *E. coli* are marked by blue circles; Bottom left: BSA-treated cellulose; Bottom right: Untreated cellulose.

Determination of synergism effects with xylanase on birch wood xylan

The measurement of released xylose from birch wood xylan after SWO1 or BSA incubation in interaction with xylanase showed a slightly increased, but not significant, degradation of xylan when incubated with SWO1 in comparison to the BSA-reference. The synergism-factor (SF) would be 1.047. By way in contrast, we would like to refer to Gourlay et al. (2013) [52], who reported an SM of 2.75 and higher with other xylanases used in combination with SWO1 on steam pretreated corn stover.

Determination of synergism effects of SWO1 with SVG on natural cellulose-comprising substrates

D. glomerata grass

After 164 h of incubation with SWO1 and SVG the sample was dissolved to a great extent (Fig 29). Also, the sample treated with BSA and SVG showed vast degradation. Confirming to the result that SWO1 shows a slight synergism with SVG, the image shows a greater break-down than the BSA-sample.

Figure 29 Grass incubated with SWO1 and SVG. From left to right: SWO1 and SVG, BSA and SVG, Buffer;

Undefined grass

Attempts to prove synergism of SWO1 and SVG on natural substrates, if not on pure cellulosic materials, were a success on undefined grass, which was picked from outside the institute (Fig 30). After 72 h the highest SF of 1.66 was obtained, followed by an SF of 1.36 after 120 h.

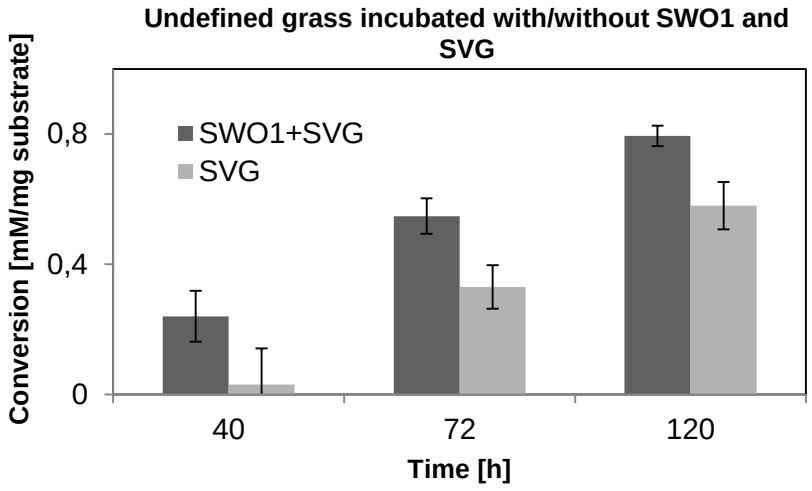

Figure 30 Conversion of 9 mg undifined grass incubated with 0.18 µM SWO1 and 2 µg SVG.

Onion epidermis

Onion epidermis incubated with SVG and SWO1 did not show different results from the SVG reference (Fig 31). Alterations detectable in the image were due to a different focus and all in all, the inspection of a number of images brings us to the conclusion that SWO1 did not show a visible synergism effect with SVG on onion epidermis.

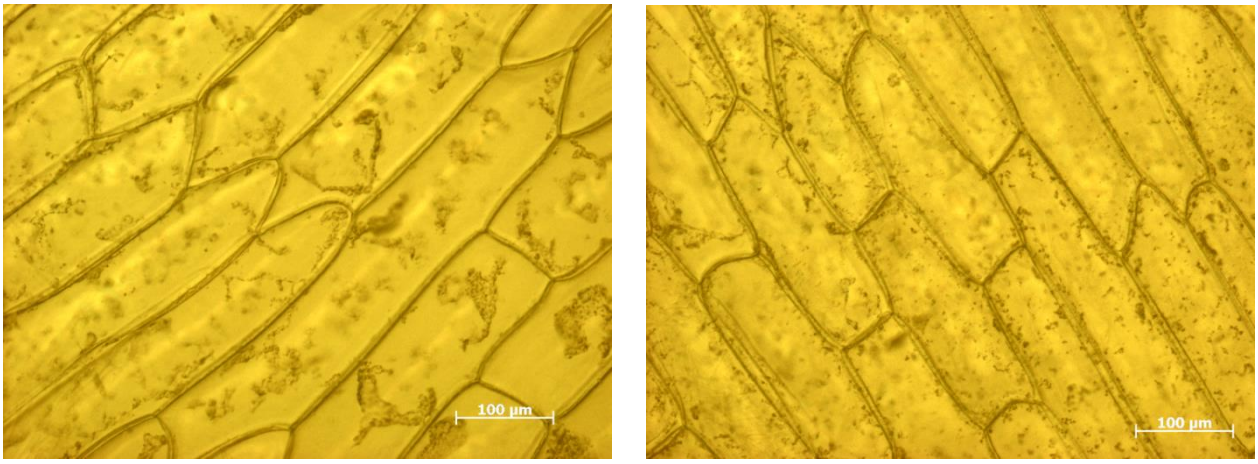

Figure 31 Onion epidermis incubated with 10 µg/ml SVG and/without 0.4 µM SWO1 for 48 h. Left: SWO1 + SVG; Right: SVG.

Atomic force microscopic measurements

In situ imaging of MACS breakdown by SVG – subsequent to SWO1-treatment – resulted in a number of images disclosing different information. This section shows a minor selection of the obtained data. Fig 32 shows the three-dimensional structure of a MACS surface. In the middle a cellulose crystal is clearly visible. Fig 33 and Fig 34 depict the same surface as two-dimensional height image and phase image, respectively. The phase image gives information about the composition of a surface [81]. This again illustrates the difference between amorphous and crystalline cellulose. The latter one is marked by a blue cross in Fig 34. Fig 35 shows the same three-dimensional structure of MACS after 3.5 h of SVG incubation, while Fig 36 shows the two-dimensional height profile at the same time point.

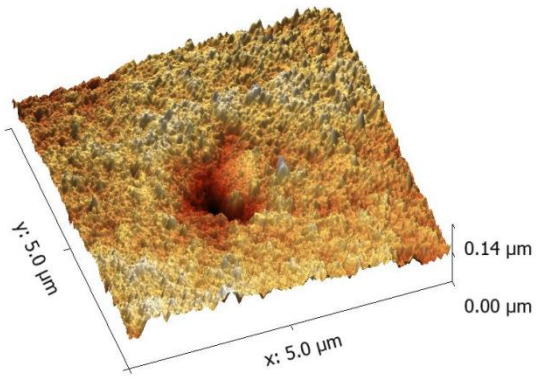

Figure 32 Three-dimensional profile of MACS surface after SWO1 treatment and before SVG incubation. In the middle is a cellulose crystal visible

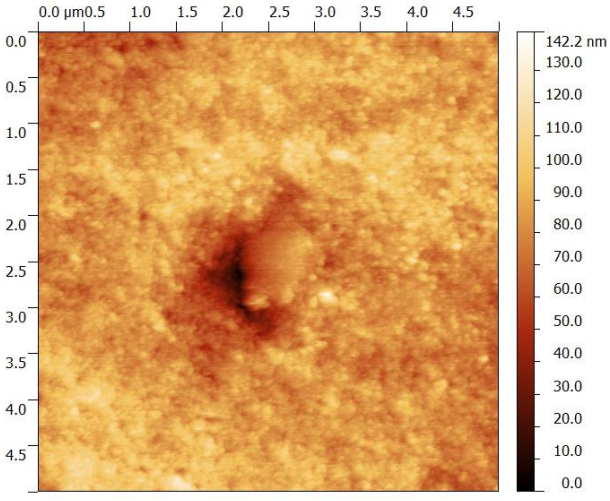

Figure 33 Two-dimensional profile of MACs surface after SWO1 treatment and before SVG incubation.

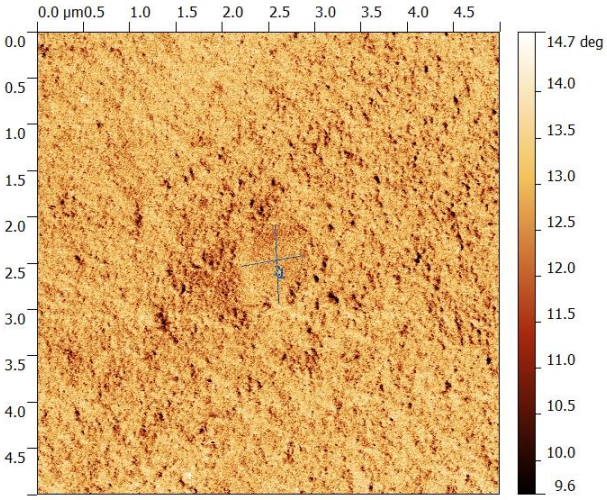

Figure 34 Two-dimensional phase image of MACS. The different composition of the substrate is clearly visible. The blue cross marks a cellulose crystal.

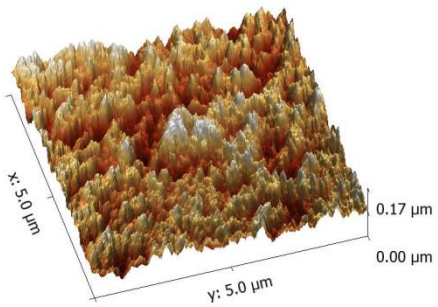

Figure 35 Figure 5 Three-dimensional profile of MACS surface after SWO1 treatment and 3.5 h of SVG incubation. The surface is vastly degraded. In the middle is a cellulose crystal still visible.

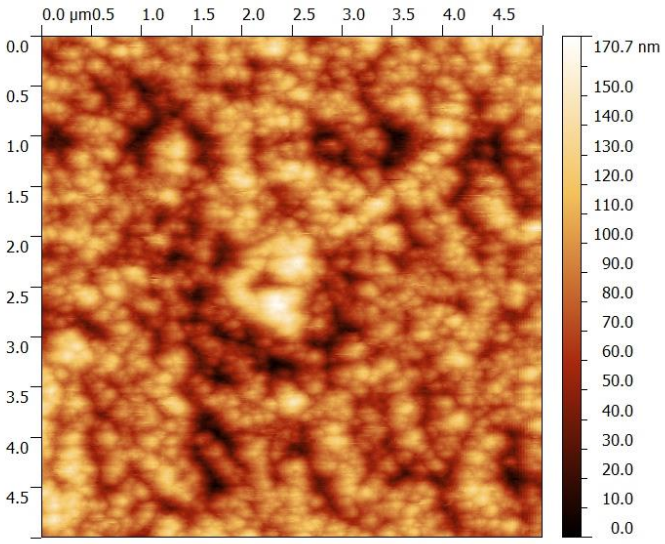

Figure 36 Figure 6 Two-dimensional profile of MACs surface after SWO1 treatment and after 3.5 h of SVG incubation.

The surface of MACS was also investigated by AFM before and after incubation with SWO1(Fig 37 and Fig 38). Although the image itself looks different, later investigations show that the height distribution is not changed by SWO1.

Another investigation with MACS containing no crystal was carried out solely with SVG. The images before (Fig 39) and after SVG addition (Fig 40) show a vast degradation of the amorphous cellulose

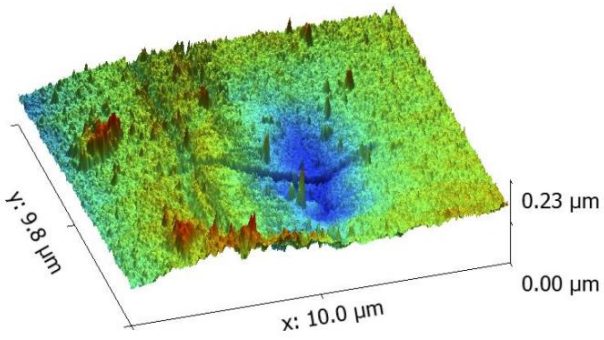

Figure 37 Three-dimensional height profile of MACS surface before incubation with SWO1.

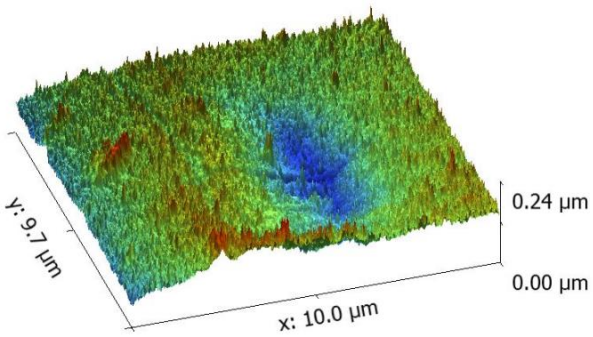

Figure 38 Three-dimensional height profile of MACS surface after incubation with 0.4 µM SWO1 for 24 h.

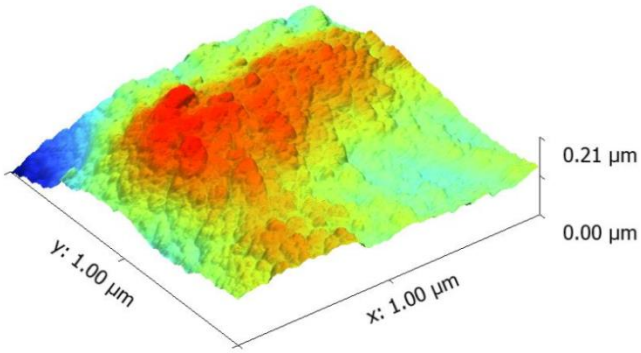

Figure 39 Three-dimensional profile of MACS surface before SVG incubation.

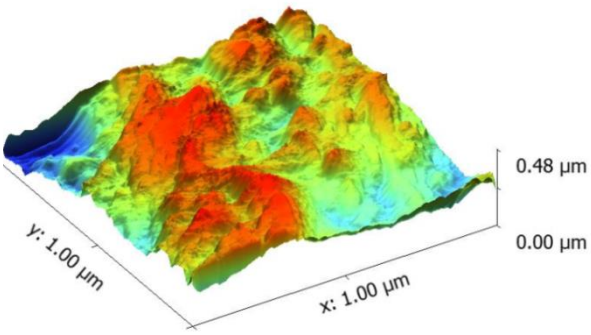

Figure 40 Three-dimensional profile of MACS surface after 0.4 h of SVG incubation.

Conclusion

SWO1 could be successfully purified with ion-exchange chromatography and, more effectively, with affinity chromatography. SWO1 shows binding affinities to Avicel, lignin and xylan and it exhibits the highest affinity for the latter one and an order of magnitude higher loading capacity for xylan and lignin in comparison to Avicel.

Moreover, SWO1 has the function to release a minor portion of reducing sugars from cellulosic substrates and β-glucan. Surprisingly, but conforming with the literature [64], SWO1 has the ability to effectively degrade cellotetraose.

Additionally, our data demonstrate that *T. reesei* SWO1 neither imposes amorphogenesis nor any other kind of structural alteration on pure cellulosic substrates. These findings were confirmed visually by AFM-measurements and additionally by WAXS. Correspondingly, no synergism with fungal cellulases on pure cellulosic substrates was detectable, though this finding stands in contrast to results found in the literature [51]. Most of the images taken were low quality and it was difficult to determine alterations induced by SWO1. Nevertheless, sharp images from SWO1 incubated onion epidermis did also not show swelling or an amorphogenesis

effect. We propose that SWO1 does not have an effect on onion cell walls that are light microscopic obtainable.

However, results, indicating that SWO1 might synergize with fungal cellulases on non-treated natural substrates, e.g. grass, lead us to the conclusion that the function of SWO1 is not targeted on pure cellulosic substrates, but rather reveals its function when exposed to natural substrates with a specific macroscopic varied structure confirming with root-colonization concepts in the literature [68,69].

References

70. Novy V, Longus K, Nidetzky B. From wheat straw to bioethanol: integrative analysis of a separate hydrolysis and co-fermentation process with implemented enzyme production. Biotechnol Biofuels. 2015;8: 46. doi:10.1186/s13068-015-0232-0

71. Esterbauer H, W S, Labudova I, Hermann A, Hayn M. Production of Trichoderma Cellulase in Laboratory and Pilot Scale. Bioresour Technol. 1991;36: 51–65.

72. Walseth CS. The influence of the fine structure of cellulose on the action of cellulases. Tech Assoc Pulp Fiber Ind. 1952;35: 228–233.

73. Eibinger M, Bubner P, Ganner T, Plank H, Nidetzky B. Surface structural dynamics of enzymatic cellulose degradation, revealed by combined kinetic and atomic force microscopy studies. FEBS J. 2014;281: 275–90. doi:10.1111/febs.12594

74. Beckham GT, Matthews JF, Bomble YJ, Bu L, Adney WS, Himmel ME, et al. Identification of Amino Acids Responsible for Processivity in a Family 1 Carbohydrate-Binding Module from a Fungal Cellulase. J Phys Chem B. 2010;114: 1447–1453.

75. Boraston AB, Bolam DN, Gilbert HJ, Davies GJ. Carbohydrate-binding modules : fine-tuning polysaccharide recognition. Biochem J. 2004;382: 769–781.

76. Pinto R, Moreira S, Mota M, Gama M. Studies on the Cellulose-Binding Domains Adsorption to Cellulose. Langmuir. 2004;20: 1409–1413.

77. Raghothama S, Simpson PJ, Szabó L, Nagy T, Gilbert HJ, Williamson MP. Solution Structure of the CBM10 Cellulose Binding Module from Pseudomonas. Biochemistry. 2000;39: 978–984.

78. Mattinen M, Kontteli M, Kerovuo J, Linder M, Annila ART, Lindeberg G, et al. Three-dimensional structures of three engineered cellulose-binding domains of cellobiohydrolase I from Trichoderma reesei. Protein Sci. 1997;6: 294–303.

79. Shoseyov O, Shani Z, Levy I. Carbohydrate binding modules: biochemical properties and novel applications. Microbiol Mol Biol Rev. 2006;70: 283–95. doi:10.1128/MMBR.00028-05

80. Vaaje-Kolstad G, Horn SJ, van Aalten DMF, Synstad B, Eijsink VGH. The non-catalytic chitin-binding protein CBP21 from Serratia marcescens is essential for chitin degradation. J Biol Chem. 2005;280: 28492–7. doi:10.1074/jbc.M504468200

81. Scott WW, Bhushan B. Use of phase imaging in atomic force microscopy for measurement of viscoelastic contrast in polymer nanocomposites and molecularly thick lubricant films. Ultramicroscopy. 2003;97: 151–69. doi:10.1016/S0304-3991(03)00040-8

Appendix 2 – *Fusarium solani pisi* Cutinase expressed in *E. coli* TOP 10 and *E. coli* Origami B (DE3)

Introduction

The successful folding of heterologous expressed proteins in *Escherichia coli* depends on a variety of factors. In addition to enzymes that actively change the conformation and chaperons that stabilize the protein during its folding [82,83], the environment of the protein is of vast importance [84]. Environmental stress can lead to misfolding and degradation of the newly translated protein [84]. Especially the formation of disulfide bonds within the protein is a process determined by the redox-potential of the cytoplasmic environment [85]. There are two pathways that are essential for the reductive property of the cytoplasm: the thioredoxin and the glutaredoxin pathway. In nature they play an important role in the reduction of disulfide bonds in proteins that may form after translation, which are mostly undesirable for cytoplasmic enzymes. The pathways involve NADPH, thioreductase and thioredoxin or glutareductase and glutaredoxin, respectively [85]. By silencing the two genes *trxA* and *gor* encoding these enzymes, disulfide bond formation is no longer reversed, because of i) the lack of reducing enzymes, ii) thioredoxin stays oxidized, by that turning the cytosol into an oxidative environment and iii) glutaredoxin loses its reducing function due to the glutareductase-knock out [86]. This circumstance promotes the utilization of the cytosol for the accumulation of heterologous disulfide-bond containing proteins, which is beneficial for many proteins. Especially, when a secretion into the naturally oxidative periplasm is inconvenient or results in a low yield [86]. Since double mutants (trxA-, gor-) are not viable, they contain a mutated cysteine-dependent peroxidase, which takes over the role of reducing disulfide bonds without significantly altering the oxidative characteristic of the cytosol [87,88]. These strains are commercially available at

Novagen and they are broadly applied for expression of disulfide-containing proteins in the laboratory.

Ribitsch et al. (2013) [89] fused a *T. reesei* disulfide-comprising cellulose-binding domain family I (CBDI) connected via a linker to cutinase I. Cutinase I from *T. cellulosilytica* is a serine esterase that hydrolyses primary alcohol esters, the main linkage of cutin [90] and has a molecular weight of 28 kDa (UniProt). Some plant pathogens are solely dependent on cutin as a carbon-source [91]. Therefore, they have developed special enzymes that are able to efficiently degrade cutin, like the *Fusarium solani pisi* cutinase or the *Thermobifida cellulosilytica* cutinase 1 [91–95]. Cutin can be ubiquitously found covering cell walls of higher plants. It is part of the protective system of the plant against influences by the environment like UV-radiation and comprises the first barrier to pathogenic attack [92,96]. It mainly consists of esterified fatty acids with a length of 16 or 18 carbon-atoms, which are hydroxylated and epoxy hydroxylated [95,97]. Primary alcohols form a net of cross-linked ester-bonds with secondary hydroxyl groups, by that establishing the polymeric network of cutin [98].

To enhance its hydrolytic activity on ester-bonds of polyethylene terephthalate (PET) Ribitsch et al. (2013) [89] fused CBDI connected via a linker to cutinase I. CBDs have the property to highly increase the binding capability of enzymes on the polymeric substrates [75] and moreover, to interfere with the recalcitrant structure of cellulose by that making it more accessible to hydrolytic enzymes [41,44,76,79]. CBDI from *T. reesei* constitutes two disulfide bonds between cysteine 485-502 and 496-512 (UniProt), which are essential for its binding function. In this study we aimed to express the Thc_CutI fusion construct in a disulfide bond promoting organism in comparison to standard expression hosts to evaluate, whether it would be possible to yield a higher portion of cellulose-binding enzymes.

Materials and Methods

Isolation of the Thc_CutI construct and preparations for inserting it into pET22b(+)

The construct *Thermobifida cellulosilytica* Cutinase I with a linker connected to a *Trichoderma reesei* CBH I CBD (Thc_CutI) in an *E. coli* BL21 was friendly provided by Ao.Univ.-Prof. Dipl.-Ing. Dr.techn. Gübitz and his group at University of Natural Resources and Life Sciences, Vienna [89]. First, the Thc_CutI-containing plasmid pET26b(+) was isolated from *E. coli* BL21 with the GeneJET Plasmid Miniprep Kit (Fermentas Life Sciences). To isolate Thc_CutI from pET26b(+) and at the same time to amplify it, a PCR with Thc_CutI specific primers was carried out. They were constructed in SerialCloner and manufactured by Sigma Aldrich. The PCR was carried out using a Dream Taq-Polymerase (5 U/ml, ThermoScientific), Kit (ThermoScientific) and the PCR cycler icycler (BIO-RAD) under standard PCR conditions. The amplified Thc_CutI construct was isolated with the NucleoSpin Gel and PCR Clean-up Kit (Macherey-Nagel). A restriction enzyme digestion was carried out with Not1 FastDigest (ThermoScientific) and Nde1 (10 U/µl, Fermentas) as a last step before the ligation into the host plasmid pET22b(+) (Novagen). The sequence product was verified by sequence analysis (LGC Genomics).

Amplification of pET22b(+) and preparation for insertion of Thc_CutI

For the amplification of the host vector pET22b(+), it was transformed into *E. coli* JM109, a well-established strain for the enrichment of plasmids. 1 µl of isolated pET22b(+) was transferred to 100 µl of *E. coli* JM109 on ice and the transformation was carried out with the MicroPulser electroporator (BIO-RAD) using the *E. coli* transformation program. Directly after the electroporation the cells were transferred into 1 ml of pre-warmed LB medium and were incubated for 1 h at 37 °C and 350 rpm on a thermomixer (Eppendorf). Subsequently, the cells were plated on LB agar containing kanamycin and put into a B6060 heating chamber (Heraeus)

at 37 °C overnight. The amplified pET22b(+) was again isolated with a purification kit. Then pET22b(+) was treated with Not1 and Nde1 and dephosphorylated with Fast Digest Thermophile Alkaline Phosphatase (1 U/µl, ThermoScientific) and following the manufacturer's instructions. Eventually, the cut and dephosphorylated product was isolated with a purification kit and was verified with an agarose electrophoresis.

Ligation of Thc_CutI and pET22b(+), amplification in *E. coli* JM109 and isolation of Thc_CutI_pET22b(+) construct

The ligation of Thc_CutI and pET22b(+) was carried out with T4 DNA ligase (5 U/µl, ThermoScientific) using a T4 DNA ligase kit (ThermoScientific) in a 2 h incubation at 22 °C and 300 rpm. The ligation was stopped at 65 °C for 5 min. The Thc_CutI_pET22b(+) construct was isolated with a purification kit and its integrity was verified by sequence analysis.

In a next step *E. coli* JM109 was transformed with the Th_CutI_pET22b(+) construct, plated and purified analogous to sub-chapter *Amplification of pET22b(+) and preparation for insertion of Thc_CutI.*

Transformation of Thc_CutI_pET22b(+) into *E. coli* strains TOP10 and Origami B (DE3), fermentation and isolation of Thc_CutI+CBM

The isolated Thc_CutI_pET22b(+) construct was transformed into *E. coli* TOP10 and Origami B analogous to sub-chapter *Amplification of pET22b(+) and preparation for insertion of Thc_CutI*. Cells of transformed TOP10 strain were plated on ampicillin-containing (amp, ROTH) LB agar, while cells of transformed Origami B were plated on kanamycin- (kan, ROTH), tetracycline- (tet, Fluca) and amp-containing LB agar, since Origami B has an intrinsic kanamycin- and tetracycline-resistance. The plates were incubated at 37 °C overnight in a heating chamber. The next day, selected transformants were again plated on amp- and kan-, tet- and amp-containing LB agar and incubated at 37 °C overnight. The growing cultures were used for pre-cultures of

the upcoming fermentation, for plating them on new agar plates as backup and storage at 4 °C and for a sequence analysis of Origami B Thc_CutI. Two 50 ml baffled flasks per strain were incubated containing the corresponding antibiotics. They were incubated at 37 °C at 110 rpm overnight. The cells in the pre-cultures were grown to an OD_{600} of 1.6, measured with a C08000 Cell Density Meter spectrophotometer (WPA biowave) and then 1.6 ml were transferred to eight 250 ml baffled flasks per strain, again containing the corresponding antibiotics. The main cultures were grown to an OD_{600} of 0.6 after seven hours at 37 °C and 110 rpm in a heating chamber and eventually were inoculated with IPTG. After that, the cultures were incubated at 18 °C and 150 rpm overnight for the Thc_CutI+CBM production. The production was stopped at 4 °C for 10 min in the cooling chamber and the cells of each strain were harvested by centrifuging for 20 min and 5000 rpm at 4 °C. The pellets were resuspended in 60 ml of 50 mM TRIS-HCl, 15 mM NaCl and a pH of 7.5 (lysis buffer) and were immediately broken up by sonification. Solids were removed by centrifugation for 45 min at 13.000 rpm and 4 °C.

For the isolation of Thc_CutI+CBM an affinity-chromatography was used. Two systems for the isolation were employed, a Duoflow system and an ÄKTA FPLC with a UPC-900 detector, a P-920 pump and a FRAC-900 fraction collector (Amersham Biosciences). Both systems were operated under similar conditions, using a copper-chelate column for the HIS-tagged Thc_CutI+CBM and a stepwise increase of 50 mM TRIS-HCl, 15 mM NaCl, 300 mM imidazol at a pH of 7,5 (elution buffer). Several fractions of the eluate were collected for the activity assessment.

Activity analysis of *E. coli* TOP10 and Origami B Thc_CutI+CBM

The activity of Thc_CutI+CBM from *E. coli* TOP10 (CutI_TOP) and Origami B (CutI_ORB) was evaluated with para-Nitrophenylacetate (pNPA). The reaction could be traced *in-situ* with a DU 800 spectrophotometer (Beckman Coulter) when starting 970 µl lysis buffer, 20 µl pNPA – 250 mM dissolved in DMSO – with 10 µl samples of different concentrations or buffer for the blank.

Measurements were carried out after adjusting the buffer of the samples with lysis buffer by centrifuging in polyethersulfone filter spin columns (Vivaspin 6, Sartorius AG) to avoid any inference of imidazole from the elution buffer in the reaction. Also, to measure the binding capacity of the protein products, 2-8 µM of protein were incubated with 10 mg/ml Avicel for 24 h at 22 °C and 300 rpm on a thermomixer. After this the samples were centrifuged at 13.000 rpm for 5 min and the activity of the supernatant was spectrophotometrically evaluated and compared to the activity of not incubated protein.

Results and Discussion

Sequence analysis of Thc_CutI_pET22b(+) construct

There were two sequence analyses carried out, each one following essential steps of the study – after the ligation of Thc_CutI into pET22b(+) and after the growth of *E. coli* Origami B containing the construct. Both of them proved to be successful and to contain unaltered components of Thc_CutI.

Purification of CutI_TOP and CutI_ORB

The purification by a Duoflow system was straight forward, reproducible and yielded in a portion of CutI_ORB and CutI_TOP. Fig 40 and Fig 41 show typical Duoflow chromatographs of Origami- and BL21-steming protein products. The blue circles indicate the isolated fraction. Nevertheless, after some troubles with one of the Duoflow pumps, all further purification was done on an ÄKTA system employing the same copper-chelate column, though slightly altered elution conditions. Fig 42 and Fig 43 show typical chromatographs of ÄKTA Origami- and TOP10-steming protein products. Again, the blue circles indicate the isolated product.

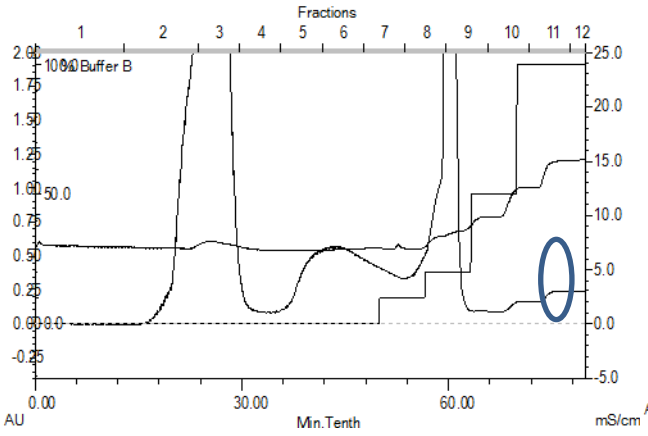

Figure 41 Typical Duoflow chromatograph of *E. coli* Origami cell lysate. The blue circle indicates the fraction with cutinase 1.

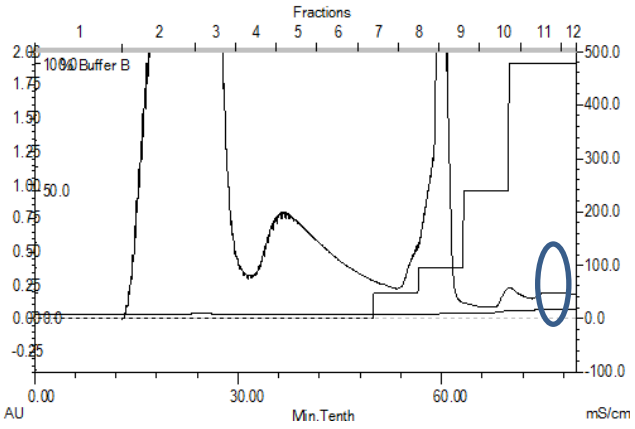

Figure 42 Typical Duoflow chromatograph of *E. coli* TOP10 cell lysate. The blue circle indicates the fraction with cutinase 1.

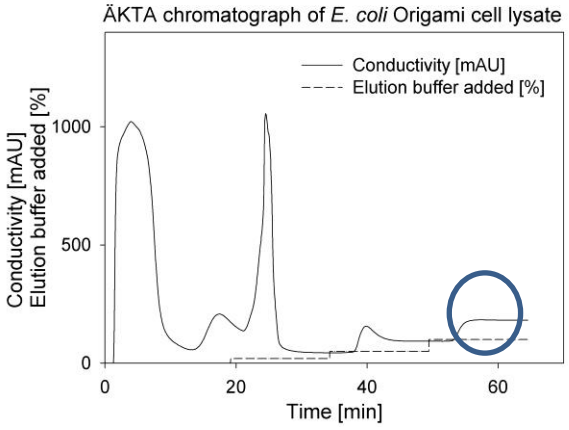

Figure 43 Typical ÄKTA chromatograph of *E. coli* Origami cell lysate. The blue circle indicates the fraction with cutinase 1.

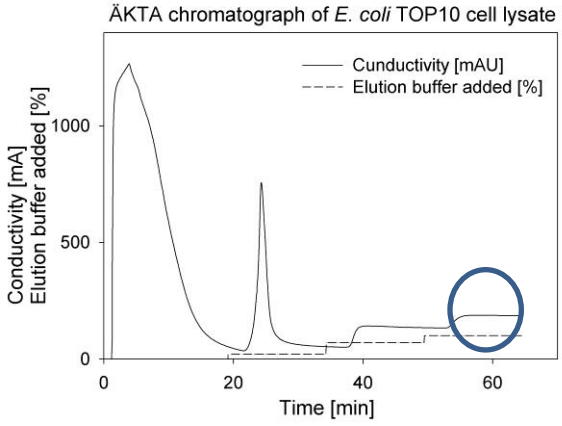

Figure 44 Typical ÄKTA chromatograph of *E. coli* Origami cell lysate. The blue circle indicates the fraction with cutinase 1.

Activity measurements

The isolated cutinase I fusion product from both *E. coli* Origami and BL21 exhibited activities comparable to the literature [89], in light of the fact that we used pNPA in contrast to Ribitsch et al. [89], who used para-nitrophenylbutyrat, which is a polymeric substrate and is therefore faster cleaved than our used pNPA. The results are

Table 2 Specific activities of Cut1_ORB and Cut1_TOP.

	CutI_ORB	CutI_TOP
Specific activity [U/mg]	42.0	43.5

Table 3 Specific activities of Cut1_ORB incubated with/without Avicel

	CutI_ORB Avicel	CutI_ORB buffer
Specific activity [U/mg]	19,7	24,6

shown in Tab 2. Nevertheless, our aim to produce a higher portion of cellulose-binding cutinase I due to the production in *E. coli* Origami B (DE3), which promotes the forming of disulfide bonds – like in the fused CBD I – could not be reached. The activity of CutI_ORB and CutI_TOP was lost by 20 % after 24 h of storage in the fridge. Attempts to prolong the stability of the fusion products included instant adjustment of the buffer, storage at 8 °C and on ice during the experiments. Experiments carried out with CutI_ORB and CutI_TOP incubated with Avicel did not show a comparable outcome and gave varied specific activities. Tab 3 shows the highest decrease of specific activity for CutI_ORB incubated with Avicel. Data always indicated that both CutI_ORB and CutI_BL21 have a binding activity, but due to the loss of activity, it was not possible to yield steady and reproducible results.

Conclusion

The aim to show an increased fraction of cellulose-binding Thc_CutI fusion constructs could not be reached. Nevertheless, the integrity of the fusion construct transformed into *E. coli* Origami was proved by DNA-sequencing, showing that further complications were not due to a partial transfer of the construct or mutations. Moreover, the isolated product showed a good specific activity and was also comparable to *E. coli* TOP10 expressed CutI_TOP. Further measurements and binding experiments were difficult due to the rapid loss of activity of both CutI_ORB and CutI_TOP. The whole process from the isolation of Thc_CutI fusion construct to activity measurements are shown in Fig 45. After extensive engagement with possible problems and several fermentations rounds, we conclude that there must be an unknown factor after the cell breakdown results into a rapid loss of the esterase activity and binding property.

Figure 45 Flow-chart of Thc_CutI+CBM production from the isolation of the DNA-sequence to activity measurements. (pET22b(+) vector image: Novagen)

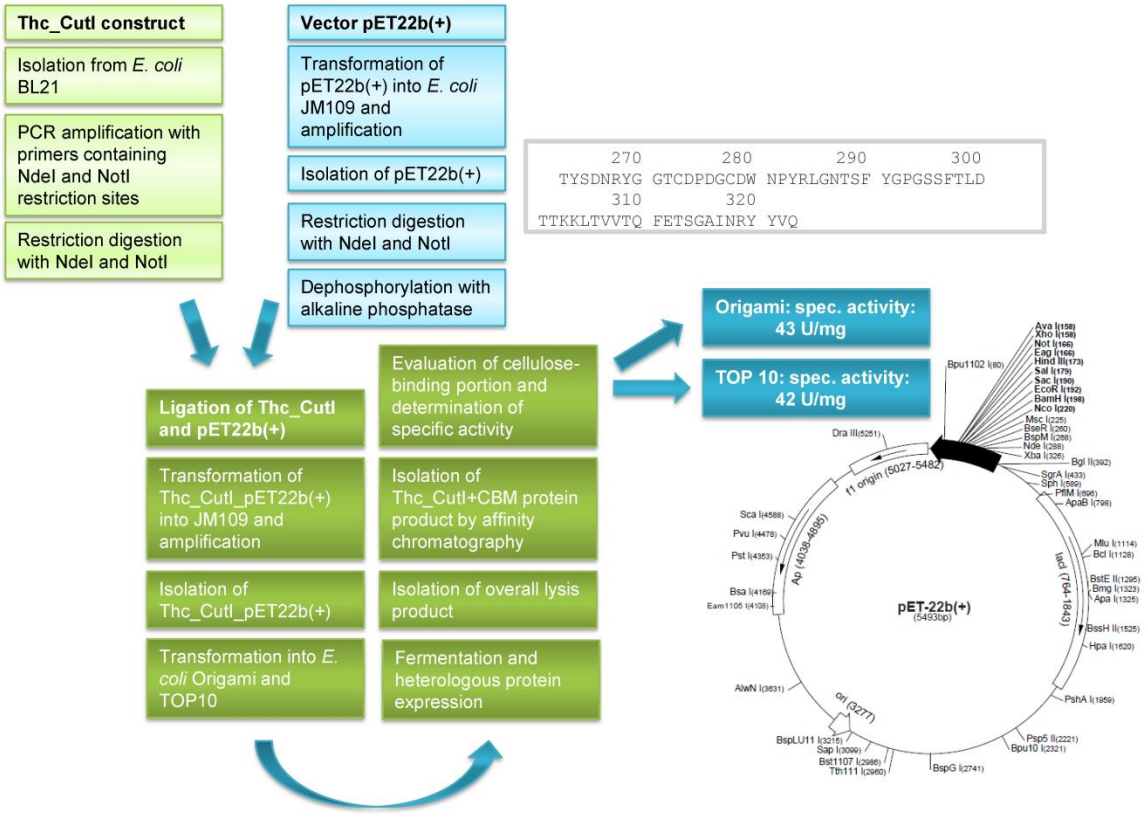

References

82. Gething M-J, Sambrook J. Protein folding in the cell. Nature. 1992;355: 33–45.

83. Dobson CM. Protein folding and misfolding. Nature. 2003;426: 884–890.

84. Baneyx F, Mujacic M. Recombinant protein folding and misfolding in Escherichia coli. Nat Biotechnol. 2004;22: 1399–408. doi:10.1038/nbt1029

85. Prinz WA, Åslund F, Holmgren A, Beckwith J. The Role of the Thioredoxin and Glutaredoxin Pathways in Reducing Protein Disulfide Bonds in the Escherichia coli Cytoplasm *. J Biol Chem. 1997;272: 15661–15667.

86. De Marco A. Strategies for successful recombinant expression of disulfide bond-dependent proteins in Escherichia coli. Microb Cell Fact. 2009;8: 26. doi:10.1186/1475-2859-8-26

87. Yamamoto Y, Ritz D, Planson A, Jönsson TJ, Melinda J, Boyd D, et al. Mutant AhpC peroxiredoxins suppress thiol-disulfide redox deficiencies and acquire deglutathionylating activity. Mol Cell. 2009;29: 36–45.

88. Faulkner MJ, Veeravalli K, Gon S, Georgiou G, Beckwith J. Functional plasticity of a peroxidase allows evolution of diverse disulfide-reducing pathways. Proc Natl Acad Sci U S A. 2008;105: 6735–6740.

89. Ribitsch D, Yebra AO, Zitzenbacher S, Wu J, Nowitsch S, Steinkellner G, et al. Fusion of binding domains to Thermobifida cellulosilytica cutinase to tune sorption characteristics and enhancing PET hydrolysis. Biomacromolecules. 2013;14: 1769–76. doi:10.1021/bm400140u

90. Martinez C, De Geus P, Lauwereys M, Matthyssens G, Cambillau C. Fusarium solani cutinase is a lipolytic enzyme with a catalytic serine accessible to solvent. Lett to Nat. 1992;356: 615–618.

91. Purdy RE, Kolattukudy PE. Hydrolysis of Plant Cuticle by Plant Pathogens . Properties of Cutinase I , Cutinase 11 , and a Nonspecific Esterase Isolated from Fusarium solani pisif. Biochemistry. 1915;14: 2832–2840.

92. Carvalho C, Aires-Barros M, Cabral J. Cutinase structure, function and biocatalytic applications. Electron J Biotechnol. 1998;1: 160–173. Available: http://www.scielo.cl/scielo.php?script=sci_arttext&pid=S0717-34581998000300006

93. Lin TS, Kolattukudy PE. Induction of a Biopolyester Hydrolase (Cutinase) by Low Levels of Cutin Monomers in Fusarium solani f . sp . pisi. J Bacteriol. 1978;133: 942–951.

94. Murphy CA, Cameron JA, Huang SJ, Vinopal RT. Fusarium Polycaprolactone Depolymerase Is Cutinase. Appl Environ Microbiol. 1996;62: 456–460.

95. Soliday CL, Kolattukudy PE. Primary structure of the active site region of fungal cutinase, an enzyme involved in phytopathogenesis. Biochem Biophys Res Commun. 1983;114: 1017–1022.

96. Heredia A. Biophysical and biochemical characteristics of cutin, a plant barrier biopolymer. Biochim Biophys Acta - Gen Subj. 2003;1620: 1–7. doi:10.1016/S0304-4165(02)00510-X

97. Kolattukudy PE. Structure, biosynthesis, and biodegradation of cutin and suberin. Annu Rev Plant Physiol. 1981;32: 539–567.

98. Fang X, Qiu F, Yan B, Wang H, Mort AJ, Stark RE. NMR studies of molecular structure in fruit cuticle polyesters. Phytochemistry. 2001;57: 1035–1042.

Addendum

Protein-sequence of *Trichoderma reesei (Hypocrea jecorina)* SWO1 (UniProt: Q9P8D0)

```
         10         20         30         40         50
MAGKLILVAL ASLVSLSIQQ NCAALFGQCG GIGWSGTTCC VAGAQCSFVN
         60         70         80         90        100
DWYSQCLAST GGNPPNGTTS SSLVSRTSSA SSSVGSSSPG GNSPTGSAST
        110        120        130        140        150
YTTTDTATVA PHSQSPYPSI AASSCGSWTL VDNVCCPSYC ANDDTSESCS
        160        170        180        190        200
GCGTCTTPPS ADCKSGTMYP EVHHVSSNES WHYSRSTHFG LTSGGACGFG
        210        220        230        240        250
LYGLCTKGSV TASWTDPMLG ATCDAFCTAY PLLCKDPTGT TLRGNFAAPN
        260        270        280        290        300
GDYYTQFWSS LPGALDNYLS CGECIELIQT KPDGTDYAVG EAGYTDPITL
        310        320        330        340        350
EIVDSCPCSA NSKWCCGPGA DHCGEIDFKY GCPLPADSIH LDLSDIAMGR
        360        370        380        390        400
LQGNGSLTNG VIPTRYRRVQ CPKVGNAYIW LRNGGGPYYF ALTAVNTNGP
        410        420        430        440        450
GSVTKIEIKG ADTDNWVALV HDPNYTSSRP QERYGSWVIP QGSGPFNLPV
        460        470        480        490
GIRLTSPTGE QIVNEQAIKT FTPPATGDPN FYYIDIGVQF SQN
```

Protein-sequence of *Thermobifida cellulosilytica* Cutinase 1 (UniProt: E9LVH8)

```
10         20         30         40         50
MANPYERGPN PTDALLEASS GPFSVSEENV SRLSASGFGG GTIYYPRENN
         60         70         80         90        100
TYGAVAISPG YTGTEASIAW LGERIASHGF VVITIDTITT LDQPDSRAEQ
        110        120        130        140        150
LNAALNHMIN RASSTVRSRI DSSRLAVMGH SMGGGGTLRL ASQRPDLKAA
        160        170        180        190        200
IPLTPWHLNK NWSSVTVPTL IIGADLDTIA PVATHAKPFY NSLPSSISKA
        210        220        230        240        250
YLELDGATHF APNIPNKIIG KYSVAWLKRF VDNDTRYTQF LCPGPRDGLF
        260
GEVEEYRSTC PF
```

Protein-sequence of linker and catalytic domain of *Trichoderma reesei (Hypocrea jecorina)* cellobiohydrolase 1 (UniProt: P62694), which was fused to *Thermobifida cellulosilytica* Cutinase 1 (UniProt: E9LVH8)

```
     270        280        290        300        310        320
TYSDNRYG GTCDPDGCDW NPYRLGNTSF YGPGSSFTLD TTKKLTVVTQ FETSGAINRY YVQ
```

Key data of *E. coli* JM109

Bacterial Strain JM109 is a useful host for transformation of pGEM® Vectors and for production of single-stranded DNA from M13 or phagemid vectors. The strain grows well and is transformed efficiently by a variety of methods. Because JM109 is *rec*A– and lacks the *E. coli* K restriction system, undesirable restriction of cloned DNA and recombination with host chromosomal DNA are prevented. The endonuclease A– mutation leads to an improved yield and quality of isolated plasmid DNA.

JM109 is deficient in β-galactosidase activity due to deletions in both genomic and episomal copies of the *lac*Z gene. The deletion in the episomal (F´ factor) copy of the *lac*Z gene (*lac*ZΔM15) can be complemented by addition of a functional α-peptide encoded by a pGEM®-Z or pGEM®-Zf Vector. If complementation does not occur, bacterial colonies are white. To maintain the F´, JM109 should be grown on minimal (M-9) media supplemented with 1mM thiamine.

Genotype: *end*A1, *rec*A1, *gyr*A96, *thi,* *hsd*R17 (r_k^-, m_k^+), *rel*A1, *sup*E44, Δ(*lac-pro*AB), [F´ *tra*D36, *pro*AB, *laq*I^qZΔM15].

Features - Benefits

- **Reliable:** Grows well and is transformed efficiently.
- **Versatile:** Useful for cloning, single-stranded DNA production, and blue/white screening.

- **High Yields of Plasmid DNA:** The endonuclease A– mutation improves yield and quality of isolated plasmid DNA.

Key data of *E. coli* TOP10

Description

One Shot® TOP10 Electrocomp™ *E. coli* are provided at a transformation efficiency of 1 x 10^9cfu/ µg supercoiled DNA and are ideal for high-efficiency cloning and plasmid propagation. They allow stable replication of high copy number plasmids. The genotype of TOP10 cells is similar to that of the DH10B™ strain, and offers the following features:
• *hsd*R for efficient transformation of unmethylated DNA from PCR amplifications

• *mcr*A for efficient transformation of methylated DNA from genomic preparations

• *lac*ZΔM15 for blue/white color screening of recombinant clones

• *end*A1 for cleaner preparations of DNA—get better results in downstream applications due to the elimination of nonspecific digestion by Endonuclease I

• *rec*A1 for reduced occurrence of nonspecific recombination in cloned DNA

Key data of *E. coli* Origami B (DE3)

Origami™ B host strains carry the same mutations in *trxB* and *gor* as the original Origami strains, except that they are derived from a *lacZY* mutant of BL21 to enable precise control of expression levels by adjusting the concentration of IPTG. Thus the Origami B strains combine the desirable characteristics of BL21, Tuner™, and Origami strains in one strain background. The mutations in *trxB* and *gor* are selectable on kanamycin and tetracycline, respectively; therefore, these strains cannot be used with plasmids that can only be selected with kanamycin or tetracycline. These strains also include the *lon* and *ompT* deficiences of BL21, which increase protein stability.

DE3 indicates that the host is a lysogen of λDE3, and therefore carries a chromosomal copy of the T7 RNA polymerase gene under control of the *lacUV5* promoter. Such strains are suitable for production of protein from target genes cloned in pET vectors by induction with IPTG.

Genotype: F^- *ompT hsd*S_B(r_B^- m_B^-) *gal dcm lacY1 ahpC* (DE3) *gor522*:: Tn*10 trxB* (Kan^R, Tet^R)

Novagen

pET-22b(+) Vector

TB038 12/98

The pET-22b(+) vector (Cat. No. 69744-3) carries an N-terminal *pelB* signal sequence for potential periplasmic localization, plus optional C-terminal His•Tag ® sequence. Unique sites are shown on the circle map. Note that the sequence is numbered by the pBR322 convention, so the T7 expression region is reversed on the circular map. The cloning/expression region of the coding strand transcribed by T7 RNA polymerase is shown below. The f1 origin is oriented so that infection with helper phage will produce virions containing single-stranded DNA that corresponds to the coding strand. Therefore, single-stranded sequencing should be performed using the T7 terminator primer (Cat. No. 69337-3).

pET-22b(+) sequence landmarks	
T7 promoter	361-377
T7 transcription start	360
pelB coding sequence	224-289
Multiple cloning sites (*Nco*I - *Xho*I)	158-225
His•Tag coding sequence	140-157
T7 terminator	26-72
lacI coding sequence	764-1843
pBR322 origin	3277
bla coding sequence	4038-4895
f1 origin	5027-5482

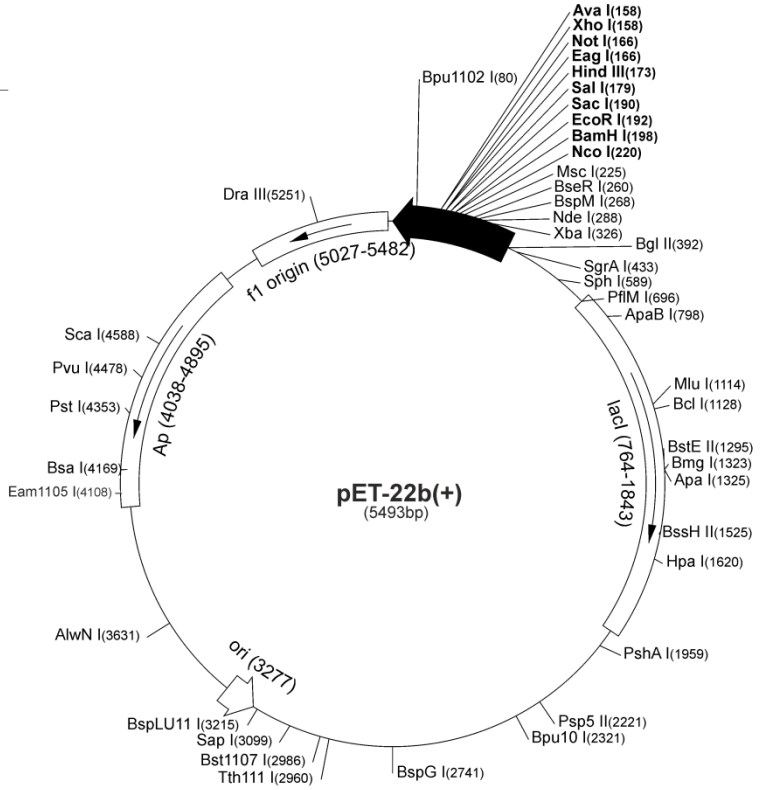

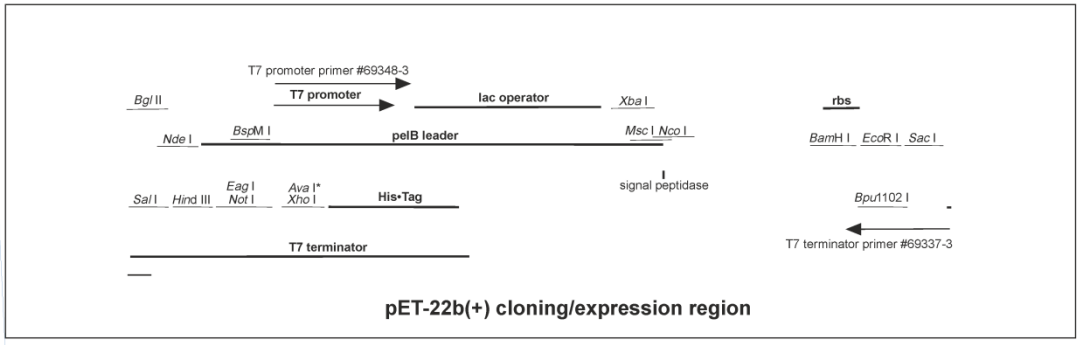

pET-22b(+) cloning/expression region

Novagen

pET-26b(+) Vector

TB071 12/98

The pET-26b(+) vector (Cat. No. 69862-3) carries an N-terminal *pelB* signal sequence for potential periplasmic localization, plus optional C-terminal His•Tag ® sequence. Unique sites are shown on the circle map. Note that the sequence is numbered by the pBR322 convention, so the T7 expression region is reversed on the circular map. The cloning/expression region of the coding strand transcribed by T7 RNA polymerase is shown below. The f1 origin is oriented so that infection with helper phage will produce virions containing single-stranded DNA that corresponds to the coding strand. Therefore, single-stranded sequencing should be performed using the T7 terminator primer (Cat. No. 69337-3).

pET-26b(+) sequence landmarks	
T7 promoter	361-377
T7 transcription start	360
pelB coding sequence	224-289
Multiple cloning sites	
(*Nco*I - *Xho*I)	158-225
His•Tag coding sequence	140-157
T7 terminator	26-72
lacI coding sequence	764-1843
pBR322 origin	3277
Kan coding sequence	3986-4798
f1 origin	4894-5349

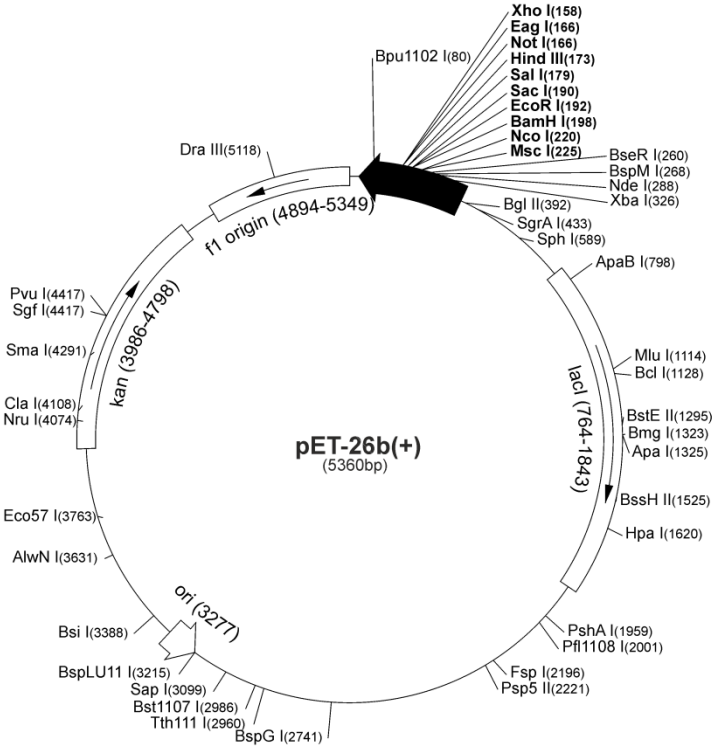

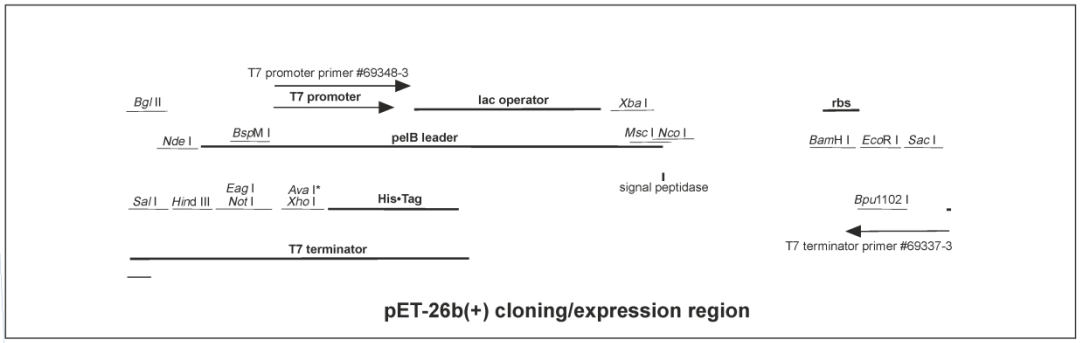

pET-26b(+) cloning/expression region